ANALYSIS AND PERFORMANCE OF AN EXPLOSIVELY DRIVEN SHOCK TUBE *

PITR-69-6

by

S. P. Gill and W. V. Simpkinson

June 1969

* This work was supported in part by Contracts No. NASw-1769 and No. NAS2-4903 with the National Aeronautics and Space Administration.

This paper was presented at the Seventh International Shock Tube Symposium held in Toronto, Ontario, Canada on June 23-25, 1969.

PHYSICS INTERNATIONAL COMPANY

3.1415926535897

2700 Merced St., San Leandro, Calif. 415/357-4610

Note — not in DDC. This copy obtained from P.I.

ANALYSIS AND PERFORMANCE OF AN EXPLOSIVELY DRIVEN SHOCK TUBE*

PITR-69-6

by

S. P. Gill and W. V. Simpkinson

June 1969

* This work was supported in part by Contracts No. NASw-1769 and No. NAS2-4903 with the National Aeronautics and Space Administration.

This paper was presented at the Seventh International Shock Tube Symposium held in Toronto, Ontario, Canada on June 23-25, 1969.

Physics International Company
2700 Merced Street
San Leandro, California 94577

TABLE OF CONTENTS

LIST OF FIGURES

SUMMARY

An explosive shock tube driver is described in which helium initially at 42 atm is shock compressed to 3.3 kbar by an implosively formed piston traveling at 6.3 km/sec. An idealized theory of explosive driver operation is presented, and the observed nonideal effects of pressure tube radial expansion, boundary-layer growth, liner jetting, preinitiation of the driver explosive, and explosive gasdynamics are described and theoretically analyzed. Performance of an explosively driven shock tube containing air at initial pressures in the range 200 to 500 μHg is discussed. Experimental data were obtained from the shock-heated air by means of high-speed rotating mirror cameras, photodiodes, time-of-arrival pins, and pressure transducers. Experiments were also conducted to determine the extent and degree of precursor ionization. Observed shock velocities were in the range 14 to 16 km/sec.

SECTION I

INTRODUCTION

The potential performance capability of explosively driven hypervelocity shock tubes, shock tunnels, and projectile launchers far exceeds the existing capability of conventional energy sources. In recognition of this potential a number of experimental programs have been conducted in recent years to determine the principal technical problems in the way of realizing this potential.

The primary difficulty in developing explosively driven systems is effectively controlling and directing the violent energy release of an explosive detonation. Various methods are currently being developed. I. I. Glass and his colleagues (References 1 and 2) utilize a spherical implosion generated by the detonation of a hemispherical liner of solid explosive. In this method the products of the explosive reaction drive an implosion wave toward the center of a hemisphere to yield essentially a point source of very high energy gas. This gas is subsequently used to accelerate a hypervelocity projectile. Seay, et al. (Reference 3), have used explosives to generate shock waves in a gas. In this method the explosive is in contact with gas in a shock tube, and a plane detonation wave in the explosive expands at its surface to drive a strong shock in the gas.

The USSR has been particularly active in explosively driven devices. Voitenko (References 4, 5, 6) has developed a device in which an explosively accelerated metal plate compresses gas in a cup-shaped cavity. Extremely high energy densities are obtained in the trapped gas, which is used to drive strong shocks in a shock tube. Zatsepin (Reference 7), Titov (Reference 8), and others have used a "cumulative charge" to drive high-velocity shock waves and projectiles. One of the authors (Reference 9) has developed an explosive shock tube in which a cloud of glass fragments jetted forward at twice detonation velocity by implosive tube collapse is used to drive a shock in low-pressure air.

The purpose of this paper is to describe a particular type of explosive driver system and its application to a hypervelocity shock tube. In its simplest form, the linear explosive driver (Figure 1) consists of a thin-walled tube containing the driver gas, usually helium. This pressure tube is surrounded by an annulus of explosive which, when detonated, progressively collapses the tube. The collapse region, traveling at detonation velocity of the explosive, completely seals the tube and acts like a high-velocity piston driving a strong shock wave into the helium driver gas.

This simple mechanical system offers great potential in controlling the release of explosive energy, and transforming the energy into a form appropriate for research in high-energy gasdynamics. Over the past few years considerable effort has been spent in investigating the detailed behavior of linear explosive drivers, and the present investigation is representative of research currently being conducted on applications of the driver to the study of hypervelocity shock wave phenomena.

SECTION II

LINEAR EXPLOSIVE DRIVER

A. IDEAL DRIVER OPERATION

In the idealized model of explosive driver operations (Figure 1) a conical piston traveling at detonation velocity is formed by the implosively collapsed pressure tube walls. This piston is assumed to seal the tube completely, so that the driver gas is forced forward to form a strong shock wave.

For the range of thermodynamic conditions achieved in explosive driver systems the helium driver gas can accurately be considered as an ideal gas with polytropic exponent $\gamma = 5/3$. The ideal driver can therefore be analyzed in terms of an ideal piston-driven shock tube with an ideal gas.

Ideally, the explosively formed piston travels at the constant detonation velocity, D, and the flow velocity of the gas is equal to the piston velocity. The Hugoniot shock jump conditions for a strong shock in ideal gas relate the shock velocity and shock pressure to the known piston velocity:

$$p_s = \frac{\gamma+1}{2} \rho_o D^2 \tag{1}$$

$$U_s = \frac{\gamma+1}{2} D \tag{2}$$

For helium driver gas $U_s = 4/3\ D$. Assuming typical values of D = 6.3 km/sec (nitromethane explosive) and $\rho_o = 7.0 \times 10^{-3}$ g/cm^3 (42 atm He), the ideal shock velocity is 8.4 km/sec and the shock pressure is 3.7 kbar.

Operation of the driver is most conveniently represented in terms of a wave diagram; i.e., a distance-time trajectory of the detonation and shock waves (Figure 2). Since the driving piston is conical, a startup process occurs before the shock front emerges ahead of the detonation. Normalizing the coordinates with respect to the diameter, d, and the detonation velocity, D, so that

$$\bar{x} = \frac{x}{d} \qquad \text{and} \qquad \bar{t} = \frac{Dt}{d} ,$$

the entire wave diagram including the startup process is ideally independent of size scaling.

A typical wave diagram for the explosive driver, including experimental data points, is shown in Figure 2. It is interesting to note that the detonation velocity increases by a factor of approximately 1.06 at a normalized time of 10; this detonation speedup is due to precompression of the explosive by the driver shock. Ideal detonation and shock wave trajectories are shown in Figure 2. If the ideal shock wave trajectory is corrected to account for the detonation speedup, the ideal shock wave trajectory coincides exactly with the experimental data. If the wave diagram is drawn from shock breakout and normalized to the pressurized nitromethane detonation velocity, the observed wave diagram is very nearly ideal. Experimental results are shown for drivers differing in size by a factor of 6; the close coincidence of the normalized data justifies the idealized concept of driver operation as a simple mechanical system.

Driver efficiency is defined to be the fraction of chemical energy in the explosive converted into kinetic and internal energy of the driver gas. The rate at which the explosive energy is released is CDE, where C is the explosive mass per unit length and E is the specific chemical energy. Similarly, the rate at which energy of the driver gas is increased is $GU_s(e_s + \frac{1}{2} D^2)$, where G is the gas mass per unit length in the unshocked gas and e_s is the specific internal energy of the shocked gas. From the shock jump conditions for a strong shock wave $e_s = \frac{1}{2} D^2$ and $U_s = \frac{\gamma+1}{2} D$. The efficiency, ϵ, of energy conversion is therefore given by

$$\epsilon = \frac{\gamma+1}{2} \frac{G}{C} \frac{D^2}{E} \tag{3}$$

in a helium driver using nitromethane explosive $D^2/E = 8.85$ and $\epsilon = 11.8\ G/C$.

Energy conversion efficiency is limited by a number of nonideal phenomena that affect driver performance, not the least of which is that at

sufficiently high shock pressures the explosively formed piston fails to seal the tube. The explosive driver used in the hypervelocity shock tube experiments described in this paper has an ideal efficiency of 12% and a measured efficiency in excess of 7%. Efficiencies of up to 20% have been obtained in some advanced designs. It should be noted, however, that efficiency of energy conversion is not necessarily a dominant factor in explosive driver systems. For example, nitromethane, with an energy density of 4.5 MJ/kg, is a commonly available industrial solvent that can easily be obtained in large quantities. For small-scale experiments the quantity of explosive is not a significant factor, so that efficiency is of secondary importance. Only in large-scale experiments is it necessary to optimize efficiency in order to reduce the total amount of explosive.

B. NONIDEAL PHENOMENA

The ideal explosive driver is characterized by an explosive collapse process that acts as an ideal piston. In this simple view details of the driver gasdynamics and explosive collapse process are neglected. In the past few years Moore (Reference 10); Waldron, et al. (Reference 11); and one of the authors (Reference 12) have experimentally identified and analyzed several phenomena that profoundly influence the performance of explosive driver systems. For the efficient high-pressure drivers found to be most useful as energy sources, the most important phenomena have been identified (Figure 3) as pressure tube expansion, boundary-layer growth in the driver gas, preinitiation of driver explosive, and jetting phenomena. Considerable additional observations and analyses have been carried out, but are too extensive for the purposes of this paper.

1. Pressure Tube Expansion

To increase efficiency of energy transfer between the explosive and the driver gas, shock pressure is maintained at a significant fraction of explosive detonation pressure. Typical driver pressures, 3 to 15 kbar, exceed the yield strength of the driver tube, and dynamic radial expansion occurs. A flash radiograph (Figure 4) of an explosive driver indicates the expansion of the pressure tube by the driver shock, and subsequent collapse of the tube by

the explosive detonation. The amount of radial expansion of the pressure tube depends on the duration and amplitude of the pressure pulse, on the geometry of the pressure tube and explosive containment tube, and on the properties of the confining material. Tube rupture has been observed experimentally to occur between 20% and 40% radial expansion. Rupture normally causes severe disturbances in the shock trajectory, and the confinement is usually chosen to limit the maximum radial expansion to less than 20%.

Details of the pressure tube expansion are complex and difficult to estimate analytically. Transit time for the shock-induced pressure disturbance through the pressure tube, explosive layer, containment tube, and back again is the same order of magnitude as the duration of the pressure pulse. Calculations based on the limiting cases of short transit times (quasi-steady analysis) and long transit times (infinite confinement) are grossly in error. We have found it necessary to perform detailed computations of the process using a one-dimensional (radial symmetry), time-dependent computer code in which the pressure tube and confinement tube materials are accurately represented by tensor constitutive equations. These computations have been checked where possible with experimental results (Figure 5), and have been found to be of sufficient accuracy to justify confidence in the results.

Expansion of the pressure tube generates rarefactions in the shocked driver gas which modify its properties and weakens the driver shock. The complex, time-dependent effects of the pressure tube expansion on the driver performance have been calculated numerically using the quasi-one-dimensional stream tube approximation. As the wall expands, radial rarefactions are created throughout the shocked-gas region that cause the pressure to decrease nearly uniformly in the gas slug. This drop in pressure causes the shock velocity to decrease, which in turn causes the particle velocity behind the shock front to decrease. The particle velocity at the piston is of course constant and is equal to the piston velocity. Briefly, the results of these calculations indicate that radial expansion of the pressure tube generates a quasi-static reduction in pressure of the shocked-gas slug, and a subsequent weakening of the shock strength.

2. Boundary-Layer Effects

Another gasdynamic phenomenon that has an influence on driver performance is boundary-layer growth. As a result of relative motion between the shock-accelerated driver gas and the pressure tube surface, a boundary layer will be formed behind the shock front. The effect of this boundary layer on the performance of the explosive driver is similar to that observed in conventional shock tubes. The deceleration of the gas near the tube walls caused by the boundary-layer growth generates rarefactions that tend to lower the shocked-gas pressure and velocity and to attenuate the shock front. In a nonjetting driver, the boundary-layer gases appear to receive little axial acceleration in the collapse region and, as a result, these gases are trapped by the implosive collapse. This process continues until a steady state is attained and the mass flow trapped in the collapse process equals the mass flow across the leading shock. At this time the shock velocity has attenuated to the detonation velocity and the slug of shocked gas has grown to its maximum length.

The effect of boundary-layer growth on the performance of an explosive driver is shown in Figure 6. For $\bar{x} < 20$ the measured shock trajectory coincides with the ideal shock trajectory, since the boundary-layer growth is negligible. The measured shock trajectory is seen to parallel the detonation trajectory at a distance of $\bar{x} > 100$. The mass flow entering the shock is equal to the mass trapped by the liner collapse process, and the shocked-gas length remains stationary.

Mirels (Reference 13) has investigated the growth of shocked-gas length in a conventional pressure-driven shock tube. The basic assumption underlying his work is that boundary-layer gas behind the shock front flows around the driver gas interface. The resulting loss diminishes shocked-gas length. The same analysis is applicable to an explosive driver if the assumption is made that boundary-layer gas is trapped in the collapse process.

Mirels' calculation of maximum shocked-gas length--the length at which mass flux in the boundary layer equals mass flux through the shock

front--exceeds the observed maximum length by a factor of two. This discrepancy is probably due to inadequate data on the transport properties of helium at high temperatures and pressures. However, when the theoretical steady-state value is adjusted to fit experimental data, the predicted growth rate greatly underpredicts the observed rate of growth of shocked-gas length (Figure 7). This discrepancy appears to come primarily from Mirels' assumption of quasi-steady flow.

In order to improve the boundary-layer predictions, a calculation was performed using a quasi-one-dimensional computer code. The explosive piston was assumed to be ideal except for a boundary-layer-induced leak rate given by

$$V = V_m \left(\frac{\ell_x}{\ell_m} \right)^{4/5} \tag{4}$$

Here ℓ_x is the shocked-gas length at shock position x, and V_m is the leak velocity corresponding to the maximum shocked-gas length ℓ_m. In this calculation rarefaction waves caused by the leak overtake and attenuate the shock. Results of these calculations agree well with experiment (Figure 7).

3. Preinitiation of Driver Explosive

Expansion of the pressure tube by driver shock pressures in the range 3 to 15 kbar exposes the explosive to transient high pressures, and under certain circumstances the explosive can detonate prematurely. Nitromethane has been the preferred explosive in explosive drivers for several years, primarily because it is classed as an industrial solvent and is easily available in large quantities. Nitromethane drivers were used for some time without any apparent problem arising from exposure to high pressure, but as driver systems were scaled to larger sizes, apparent irregularities in the late-term behavior of the detonation trajectory were noticed. Ionization pins used to detect passage of the detonation wave reported early, and indicated a possible acceleration of the detonation wave to a velocity roughly equal to the shock velocity in the driver. The ionization pin readings were erratic, but clearly implied some energy release when the nitromethane was exposed to pressures of approximately 5 to 10 kbar for periods in excess of 75 μsec.

Initiation of homogeneous nitromethane at shock pressures in excess of 80 kbar is at least fairly well understood at present (Reference 14). The initiation process consists of three phases: (1) compression and shock heating of nitromethane to temperatures in excess of 1000°K, (2) a chemical induction period governed by an Arrhenius reaction rate leading to runaway thermochemical decomposition of the explosive, and (3) a rapid increase in pressure and temperature behind the shock front and acceleration of the shock into a self-sustaining detonation. Calculations of the chemical induction time for homogeneous nitromethane compressed to 10 kbar indicate an expected induction time of 10^{7} sec, far in excess of the observed times on the order of 10^{-4} sec. It was clear from this analysis that the observed initiation phenomenon was based on a physical mechanism substantially different from that observed at pressures in excess of 80 kbar.

After an experimental and analytical investigation too extensive to report in this paper, the initiation mechanism was identified as the compression of minute air bubbles trapped in the liquid nitromethane. The initiation process proceeds by compression-heating of the trapped air to temperatures on the order of 3000°K. The compression temperature depends on the equation of state, and it was necessary to use real-air thermodynamic tables to agree with experiment. The temperature of the nitromethane at the liquid-gas interface rises to temperatures on the order of 1000°K by heat conduction, and a complex thermochemical heat transfer process begins. For bubble dimensions smaller than approximately 10^{-4} cm, heat loss by conduction exceeds heat input by chemical decomposition, and the disturbance is quenched. For larger bubble dimensions the high surface temperature leads to runaway thermal decomposition with a characteristic chemical induction time. Calculations of chemical induction time for real air bubbles are shown in Figure 8, and indicate an induction time at 10 kbar on the order of 10^{-4} sec.

Dependence of the initiation mechanism on temperature rise in trapped air bubbles implies that the observed preinitiation phenomenon can be suppressed by prepressurization of the explosive. Temperature rise in a compressed gas depends on the initial pressure, and increasing the initial

pressure decreases the final temperature. The induction time is dependent on temperature, and a small change in nitromethane interface temperature greatly increases initiation time. Calculations for an initial pressure of 40 atm (Figure 8) indicate an increase in induction time by five orders of magnitude.

Prepressurization of the explosive driver has been experimentally verified as a means of suppressing preinitiation phenomena, and at present there appears to be no known limit in scaling nitromethane explosive driver systems to very large sizes for aerodynamic applications.

4. Jetting Phenomena

At sufficiently high implosive collapse velocities, the imploding pressure tube walls can jet forward into the driver gas (Figure 3). Jetting is essentially a dynamic phenomenon similar to splashing of a liquid. Birkhoff's classic analysis of jetting (Reference 15) assumes that impact pressures are sufficiently great to neglect material strength, so that flowing metal is treated as a liquid. In a frame of reference moving with the collapse, the process is steady state and Bernouilli's law holds:

$$h + \frac{1}{2}u^2 = \text{constant} \qquad (5)$$

where h is the enthalpy and u the flow velocity in the metal pressure tube walls. This equation is essentially a statement of the First Law of Thermodynamics, and is independent of most of the complex processes occurring within the flowing metal. If the density variations induced by the flow pressures are small, then $h = p/\rho$. Substituting this expression in Equation 5, we obtain the classical Bernouilli equation for an incompressible material. At a free surface exposed to constant pressure, the velocity is constant. In the steady-state frame of reference the imploding pressure tube is initially at the detonation velocity, D, so that the emerging jet also has the velocity D. In the laboratory frame of reference the forward jet has the velocity 2D.

Following Birkhoff, the mass of the jet can be calculated by applying conservation of axial momentum. Suppose that pressure of the expanded

detonation gases and the compressed driver gas are negligible. Then the axial momentum of the pressure tube wall material flowing into the collapse region must equal the sum of the flow of vector momentum flowing out of the collapse region:

$$MD^2 \cos \alpha = M_s D^2 - M_j D^2 \tag{6}$$

Here M, M_s, and M_j are the mass per unit length of the imploding wall, the emerging slug, and the jet; α is the cone half-angle of the imploding pressure tube wall. Combining Equation 6 with conservation of mass ($M = M_s + M_j$), we obtain Birkhoff's equation for the jet mass:

$$\frac{M_j}{M} = \frac{1 - \cos \alpha}{2} \tag{7}$$

Since the cone half-angle α is typically 5° to 10°, Birkhoff's equation implies that as much as 0.8% of the wall material is jetted forward.

We have observed that jet mass can be significantly diminished by irreversible processes occurring in the flowing metal as it traverses the impact region. If an irreversible process occurs, such as plastic flow of the metal or shock deceleration, energy is transferred (according to Equation 5, expressing the First Law of Thermodynamics) from kinetic to internal energy. If the irreversible processes are minor, the velocity change is small, and the equations governing conservation of mass and momentum can be written in terms of a velocity decrement through the impact region:

Mass: $$MD = M_s D(1-\epsilon_s) + M_j D(1-\epsilon_j) \tag{8}$$

Momentum: $$MD^2 \cos \alpha = M_s D^2(1-\epsilon_s)^2 + M_j D^2(1-\epsilon_j)^2 \tag{9}$$

Solving for jet mass, M_j, we find:

$$\frac{M_j}{M} = \frac{1 - \cos \alpha - \epsilon_s}{(2 - \epsilon_s - \epsilon_j)(1 - \epsilon_j)} \tag{10}$$

Even though ϵ_s and ϵ_j may be small, total jet mass can be substantially modified. For a 10° cone half-angle, the jet mass vanishes for $\epsilon_s = 0.015$.

The relatively small irreversible effects, such as plastic flow and shock wave phenomena in the metal, can therefore have a substantial effect on jet mass.

Growth of a boundary layer in the driver gas also acts to minimize jetting. The mass of gas moving at wall velocity acts as an extension of the wall, and the metal jet is diminished by the mass of boundary-layer gas jetted forward. Jetting has been found to be a problem for explosive driver systems only for low driver pressures (less than 2 kbar), and it can usually be eliminated by reducing the velocity of the imploding pressure tube walls.

C. EXPLOSIVE DRIVER PERFORMANCE

Observed nonideal phenomena in the linear explosive driver limit its performance. At driver pressures in excess of 15 kbar the problems of pressure tube expansion, boundary-layer effects, and explosive preinitiation are excessive. At low pressures (less than approximately 2 kbar) efficiency of the driver is poor.

Explosive drivers using nitromethane explosive have been found to be particularly effective as gasdynamic energy sources for operating pressures of approximately 3 to 10 kbar. Detonation velocity ranges from 6.3 to 6.9 km/sec (depending on driver pressure), and ideal efficiency ranges from 5% to 15%.

For explosive driver systems designed to minimize the effects of boundary-layer growth and pressure tube expansion, the measured performance closely matches the ideal performance (Figure 2), and the measured efficiency is equal to the ideal efficiency. As boundary-layer effects begin to dominate, measured efficiency decreases by the amount of gas loss.

The explosive driver configuration chosen for the hypervelocity shock tube experiments is shown in Figure 9. It consists of a 5-cm i. d. steel pressure tube containing 42 atm helium, a 6-mm annulus of liquid nitromethane

explosive, and a 9.5-mm steel containment tube backed by 30 cm of concrete. The ideal driver pressure is 3.7 kbar, and ideal efficiency of the driver is approximately 12%.

The length of the driver is approximately 40 tube diameters, which indicates that boundary-layer effects are present, but not dominant (Figure 7). Calculated maximum pressure tube expansion is 15%, a value leading to slight expected degradation of performance.

Experimental performance of this explosive driver design is presented in the next section.

SECTION III

EXPLOSIVELY DRIVEN SHOCK TUBE

The purpose of the experimental investigation reported in this paper was to investigate the possibility of using a linear explosive driver to generate hypervelocity shock waves in air. A second objective of the program was to investigate the practical limitations of sophisticated diagnostic measurements in an explosive experiment. The experiments were conducted in a permanent shock tube laboratory specially designed to protect delicate instrumentation from the explosive blast wave.

Preliminary experimental results have been encouraging. Shock velocities from 14 to 16 km/sec in air at initial pressures of 200 to 500 mTorr have been achieved in a 10-cm shock tube, and the measured shock velocities compare well with theoretical performance based on an ideal driver. Instrumentation was found to be well protected from the explosive blast, and measurements of shock properties were made with a variety of instruments.

A. IDEAL SHOCK TUBE OPERATION

Operation of an explosively driven shock tube is similar to a conventional pressure-driven shock tube, except that the driver gas is traveling at a high velocity. The shock-compressed driver gas breaks a diaphragm and expands through a nozzle into the driven section, driving a strong shock into the low-pressure test gas.

The wave diagram of an explosively driven shock tube is shown in Figure 10. Regions of constant state are identified in a manner consistent with conventional shock tube notation: Region 1 identifies the unshocked test gas (usually low pressure); Region 2 is the shocked test gas; Region 3 is expanded driver gas; and Region 4 is shocked driver gas. In addition, Region 4' stands for the unshocked driver gas, and Region 4D for the driver gas after expansion from the nozzle.

Details of explosive shock tube operation differ from conventional pressure-driven shock tubes in a number of ways. Since flow behind the strong driver shock is supersonic, the unsteady rarefaction fan caused by bursting of the diaphragm is swept downstream. The first wave disturbance in Region 2 identifying the end of constant-state test time is due to a rarefaction generated by the sudden stop of the explosive piston. In a conventional shock tube the first disturbance is caused by reflection of the diaphragm opening rarefaction. Details of the calculation of rarefaction fans and test times in an explosive shock tube therefore vary considerably from a conventional shock tube, although the basic principle of operation remains the same.

For the range of conditions achieved in an explosive driver, helium driver gas can accurately be characterized as a perfect gas. Calculations of the unsteady rarefaction fans, steady expansion, and trajectory of the terminating characteristics can all be carried out analytically in terms of known driver conditions.

Conditions in the test gas are far too severe to use a perfect gas approximation. It is not necessary, however, to obtain a complete equation of state. For a strong shock wave, the Hugoniot shock relations give, in general,

$$p_2 = \frac{\rho_1 u_2^2}{1 - \frac{1}{\eta}} \tag{11}$$

where η is the density ratio across the shock. Even though η varies between 10 and 15 for air at high shock velocity (10 to 20 km/sec), the quantity $1 - \frac{1}{\eta}$ only varies between 0.90 and 0.933; i.e., the uncertainty in shock pressure is less than 4%.

For given driver conditions, the flow velocity u_2 in the driven section is obtained by determining the isentropic p_3-u_3 expansion relationship. Across the contact surface pressure and velocity are constant, so that $p_3 = p_2$ and $u_3 = u_2$. The isentropic p_3-u_3 expansion curve, combined with the p_2-u_2 shock relationship (Equation 11), suffices to determine the theoretical shock conditions in the driver tube.

The isentropic p_3-u_3 relationship can be calculated by assuming the expansion process to consist of a steady expansion through the nozzle followed by an unsteady expansion to the driven tube pressure. The perfect gas relationships for the steady expansion are (References 16 and 17):

$$\frac{u}{a_t} = M\left[1 + \frac{\gamma-1}{2}(M)^2\right]^{-\frac{1}{2}} \tag{12}$$

$$\frac{p}{p_t} = \left[1 + \frac{\gamma-1}{2}(M)^2\right]^{-\frac{\gamma}{\gamma-1}} \tag{13}$$

$$\frac{A}{A^*} = \left(\frac{\gamma+1}{2}\right)^{-\frac{\gamma+1}{2(\gamma-1)}} M^{-1}\left[1 + \frac{\gamma-1}{2}(M)^2\right]^{\frac{\gamma+1}{2(\gamma-1)}} \tag{14}$$

For the unsteady expansion

$$\frac{p}{p_t} = \left[1 - \frac{\gamma-1}{2}\frac{u}{a_t}\right]^{\frac{2\gamma}{\gamma-1}} \tag{15}$$

$$\frac{u}{a_t} = M\left[1 + \frac{\gamma-1}{2}M\right]^{-1} \tag{16}$$

Here M is the local Mach number, p the pressure, u the velocity, a the sound speed, and A the cross-sectional area of the flow. A* denotes the area for unity Mach number, and the subscript t identifies total conditions (i.e., conditions that would exist if the gas were initially at rest in the given process). Total conditions for the steady expansion process and the unsteady expansion are different, and should not be confused.

It is useful to normalize the shock tube calculations with respect to the driver velocity, u_4, and the driver shock pressure, p_4. The normalized p_2-u_2 shock relationship (Equation 11) becomes

$$\frac{p_2}{p_4} = K\left(\frac{u_2}{u_4}\right)^2 \tag{17}$$

where

$$K = \rho_1 u_4^2 / [p_4(1 - \frac{1}{\eta})] \tag{18}$$

From the strong shock relations it can easily be shown that

$$M_4 = \left\{ \frac{\gamma(\gamma-1)}{2} \right\}^{-\frac{1}{2}} \tag{19}$$

Equations 19 and 14 can be used to relate M_{4D} to the nozzle area ratio:

$$\frac{A_{4D}}{A_4} = \left\{ \frac{\gamma(\gamma-1)}{2} \right\}^{-\frac{1}{2}} \left\{ 1 + \frac{2}{\gamma} \right\}^{-\frac{\gamma+1}{2(\gamma-1)}} M_{4D}^{-1} \left\{ 1 + \frac{\gamma-1}{2} M_{4D}^2 \right\}^{\frac{\gamma+1}{2(\gamma-1)}} \tag{20}$$

Given the ratio A_{4D}/A_4, the Mach number M_{4D} in the expanded flow can be iteratively calculated.

Next, Equations 12, 13, 15, 16, and 20 can be manipulated to yield

$$\frac{p_3}{p_4} = \left\{ \frac{\left\{ \frac{\gamma+1}{\gamma} \right\}^{1/2} \left\{ 1 + \frac{\gamma-1}{2} M_{4D} \right\}}{\left\{ 1 + \frac{\gamma-1}{2} M_{4D}^2 \right\}^{1/2}} - \sqrt{\frac{\gamma-1}{2\gamma}} \frac{u_3}{u_4} \right\}^{\frac{2\gamma}{\gamma-1}} \tag{21}$$

This equation is the desired p_3-u_3 relationship for the isentropic expansion of the driver gas.

The normalized pressure-velocity curves for the expansion of helium driver gas (Equation 21) and the driven tube shock (Equation 17) are plotted in normalized coordinates in Figure 11. Intersection of these curves represents a simultaneous solution of the two equations.

Operating point in a given explosively driven shock tube is obtained by first determining the value of K (Equation 18) from the known density ρ_1 and an assumed value of η. Since η cannot be exactly determined unless the operating point is known, K must be approximated at first and then refined by iteration. However, since K varies by only a few percent over the total expected range of η, this iterative correction is usually unnecessary.

The value of K determines a particular shock pressure-velocity curve (Figure 11), and the intersection of this curve with the driver expansion curve determines the p_2-u_2 operating point. The exact value of the shock density ratio of η can then be determined from shock tables, and K updated if necessary. Shock velocity in the driver section is given by the shock relation:

$$u_s = u_2 / \left(1 - \frac{1}{\eta}\right) \tag{22}$$

Determination of ideal test time from the intersection of the terminating characteristic with the contact surface requires an integration of the characteristic trajectory through the steady nozzle expansion and the unsteady rarefaction fan in the driven section. This integration is readily carried out either numerically or graphically, but the process is tedious. Sufficient accuracy for some design purposes can be obtained by assuming that the characteristic velocity through the expansion regions is equal to the average of the velocities in adjacent regions of constant state. This analysis yields the following equation for the distance from the diaphragm at which the terminating rarefaction overtakes the contact surface:

$$\frac{L_o}{T_D} = u_3 \frac{(u_4 + a_4)(u_3 + a_3 - u_4 + 3a_4)}{a_4(u_4 + a_4 - u_3 + 3a_3)} \tag{23}$$

where L_o is the overtake distance and T_D is the driver run time.

B. EXPERIMENTAL PROGRAM

A short experimental program has been carried out to investigate the performance of a hypervelocity shock tube driven by an explosive driver. Three experiments were conducted on a 10-cm-diam. shock tube with initial air pressures ahead of the shock of 250 and 400 mTorr. The experimental program also served to investigate the possibility of decoupling the explosive blast from the shock tube and its associated instrumentation.

Of the three experiments conducted, one was performed with air at 250 mTorr initial pressure and two with pressures of 400 mTorr. These

three firings resulted in shock velocities of 14.2, 15.4, and 16.4 km/sec. The shock velocities were constant to within the precision of the measurements for the entire length of the 8-m shock tube. The observed velocities were slightly less than predicted for an ideal explosive driver.

Photographs of the shock-heated air showed the shock front to be plane. The homogeneous luminous region behind the shock front extends at least 3 cm.

Measurements of the electron conductivity ahead of the shock wave indicated appreciable ionization to a distance of 65 cm ahead of the shock front. An electron density in excess of 10^9 cm^{-3} was measured 16 cm ahead of the shock wave.

This work has demonstrated the ability of the explosive driver to generate plane shock waves moving at velocities in excess of 15 km/sec into air at densities corresponding to altitudes of approximately 60 km. The work has also demonstrated that diagnostic instrumentation, employing delicate apparatus, can successfully be applied for a permanent explosive-driven shock tube.

1. Explosive Shock Tube Laboratory

Explosively driven shock tubes present a number of experimental problems not ordinarily associated with shock tube research. One of the major problems is the necessity of decoupling the shock tube instrumentation from the destructive blast wave associated with detonation of explosive. The two simplest approaches to this problem are containing the explosive in a large steel tank, or protecting the instrumentation in a blast-proof bunker. The first method has been used with success for a variety of explosive devices, but it is practically limited to a few kilograms of explosive. If a field test site is available, the second approach allows more flexibility in explosive driver design.

Physics International Company has constructed an explosive shock tube facility at its Tracy Test Site (Figure 12) specially designed to protect sensitive shock tube instrumentation from explosive blast effects. The shock tube passes through a steel-sheathed, reinforced concrete wall into a blast-proof bunker containing the shock tube instrumentation. The shock tube and instrumentation setup are shown in Figure 13.

Personnel and remote control and recording instruments are located in a second bunker (Figure 14). The purpose of maintaining two bunkers is to eliminate the danger of shock tube rupture at the very high shock pressures possible in an explosively driven shock tube.

2. Explosive Driver Performance

The driver shock and detonation trajectories (Figure 15) were monitored by contact and ionization pins. The contact pins are closed by the shock-induced expansion of the pressure tube, and the ionization pins are short circuited by the ionized detonation products. The pins discharge capacitors on the passage of the shock front and detonation front, and these discharge pulses are monitored by a raster oscilloscope in the instrumentation bunker.

The observed detonation velocity of 6.8 km/sec is greater than ideal detonation velocity of 6.3 km/sec because of precompression of the nitromethane by the driver shock. The observed shock velocity, 7.6 km/sec, is less than either the ideal velocity of 8.4 km/sec based on ideal detonation velocity, or 9.1 km/sec based on observed detonation velocity. The difference is attributable to the nonideal effects of pressure tube expansion and boundary-layer growth discussed previously.

The initial helium pressure in the driver was 42 atm, which corresponds to a pressure of 3.7 kbar in the ideal driver. Calculated pressure based on the observed shock velocity is 3.1 kbar.

An independent measure of driver performance was obtained by monitoring driver pressure with a piezoelectric pressure transducer. The transducer was calibrated at low pressures with a static test device before

and after the shot, but it has been our experience that dynamic accuracy of the calibration is no better than ± 10%. The oscilloscope record (Figure 16) indicates an initial pressure step of approximately 2.7 kbar, followed by a slow rise over 20 μsec to a steady value of approximately 3.3 kbar. The most probable explanation for the slow rise is that driver gas in the expanded pressure tube is recompressed when it flows into the shock tube coupling section.

Observed run time in the explosive driver is 60 μsec to the start of the terminating rarefaction. Assuming an average pressure of 3.3 kbar during this period, the calculated thermodynamic efficiency of the driver is slightly greater than 7%.

3. Shock Wave Trajectory

The shock trajectory in the shock tube was determined with ion pins similar to those used in the explosive driver. The measured trajectory in Shot 121-2 (Figure 15) indicates a shock velocity of 16.4 km/sec, constant to within the accuracy of the measurements.

Three shots of the explosive shock tube were fired during the experimental program. The results are tabulated in Table I, and are compared with calculations based on an ideal driver. The agreement between the ideal calculations and experimental observations for the 400 mTorr shots are of course fortuitous, as there are a number of interacting nonideal effects present which happen to cancel each other. It is not clear at this time why the 250 mTorr shot has an unusually low velocity; driver data were not recovered on this shot, and there is the possibility of a driver malfunction.

It is interesting to note the absence of diaphragm break time usually associated with shock tubes. The measured shock trajectory in the shock tube starts no later than a few microseconds after arrival. The explosively driven shock tube has the advantage that the diaphragm can be quite thin, as it is necessary to withstand only the low initial pressure (42 atm) of the driver gas. The reflected driver pressure is 36 kbar, which is sufficiently high to destroy almost instantaneously the thin diaphragm.

TABLE I

COMPARISON OF IDEAL AND OBSERVED SHOCK VELOCITIES

a. Ideal Shock Velocities (u_s)

Initial Shock Tube Pressure(mTorr)	Velocities for Area Ratio = 4 (km/sec)
250	16.0
400	15.7

b. Observed Shock Velocities (u_s)

Shot Number	Initial Shock Tube Pressure (mTorr)	Measured Shock Velocities (km/sec)
121-1	250	14.2
121-2	400	16.4
121-3	400	15.4

4. Evaluation of Shocked-Air Conditions

One of the purposes of the experimental program was to investigate the possibility of using sophisticated instrumentation in our explosively driven shock tube. The design of the blast-proof shock tube bunker proved to be adequate in reducing explosive blast effects, and even delicate high-speed photographic equipment was successfully used.

A photographic view of the self-luminous shocked air in Shot 121-3 was taken with a high-speed rotating mirror camera (Figure 17). A clear plastic ring was inserted between flanges of the shock tube, and formed a slit-like window for viewing the shock wave. The optical image of this slit was reflected from the rotating mirror, and was focused onto 35-mm film. The speed of the rotating mirror was adjusted so that the slit image traveled at the rate of 2 km/sec on the film. The streaked slit image generates a picture of the shocked gas as it flows past a point; assuming the shock velocity to be constant, this time-resolved image is equivalent to a direct photograph of the shocked gas.

Within the resolution of the optical system, the photograph (Figure 17) indicates that the shock front is plane. It is not clear where the contact surface is located. The luminosity of the gas diminishes rapidly behind the shock due to radiative cooling, so that reduction of film exposure is not a reliable indication of the contact surface. The observed luminous region extends for at least 3 cm behind the shock front, and establishes a lower bound of approximately 2 μsec for the test time.

Photodiodes were also used to monitor the luminous plasma. The photodiodes were mounted at several stations on the shock tube wall, and were collimated by means of two 1-mm apertures separated by 43 mm. The diodes were saturated by the light output, but indicated a test time of approximately 5 μsec at a distance 6.4 m from the diaphragm.

Mirels' theory of shock tube test time (Reference 13), extrapolated to the experimental shock Mach number, predicts a test time of approximately 4 μsec. This value is well within the experimental uncertainty concerning the location of the contact surface.

Spectroscopic measurements were also conducted with a high-speed spectrograph. The measurements were exploratory in nature and fairly crude, but they did indicate the presence of metallic emission lines. The source of these metallic impurities is thought to be the boundary layer, judging from experimental data in other programs. However, it is possible that the contamination is due to metallic impurities in the helium driver gas diffusing into the shocked-air slug. Theoretical predictions based on estimates of driver contamination indicate that this is an unlikely possibility, but it is a question that can be resolved only by obtaining additional experimental data.

5. Precursor Conductivity Measurements

A four-wire conductivity probe based on Brown's design (Reference 18) was used to measure precursor conductivity in Shot 121-3. This probe (Figure 18) consists of four equally spaced bare wires exposed to the conducting plasma. A voltage is applied across the two outer conductors.

Measurement of the current, i(t), through the outer conductors and the voltage, e(t), across the two inner conductors is sufficient to determine conductivity of the plasma. The probe was calibrated by measurements in an ionic solution of soluble salts in water.

Measurable conductivity (approximately 0.02 mho/m) was observed as much as 40 μsec before arrival of the shock. At the measured shock velocity of 15.4 km/sec, this time corresponds to a distance of 62 cm ahead of the shock front. Conductivity values were converted to approximate electron density values using the well-known equations of a weakly ionized plasma (Reference 19). Electron temperature was assumed to be approximately 1 eV.

SECTION IV

CONCLUSIONS

The purpose of the experimental program described in this paper was to investigate the performance of a hypervelocity shock tube driven by a linear explosive driver, and to determine the feasibility of performing sophisticated diagnostic measurements in a permanent shock tube facility protected from the explosive blast. The shock tube facility proved to be adequately protected, and measurements of shock tube performance were made with such delicate instruments as a high-speed rotating mirror camera.

The present stage of investigation into the performance of the explosively driven shock tube is encouraging but not conclusive. Observed shock velocities were in the range 14 to 16 km/sec in air at initial pressures of 0.25 to 0.4 Torr. From the streak camera records the shock appears to be plane, and test time is approximately the maximum time predicted by Mirels' boundary-layer theory. Preliminary spectroscopic results indicate the presence of metallic contamination, but this is thought to be confined to the boundary layer. The basic performance potential of the explosively driven shock tube has been demonstrated in this program, but additional research is necessary to determine thermodynamic conditions in the shocked gas.

It is interesting to compare the performance potential of the explosively driven shock tube described in this paper with the performance of existing arc-driven and combustion-driven shock tubes. Camm, et al. (Reference 20), have described the performance of a very high performance, 80-kJ, arc-driven shock tube and a large combustion-driven shock tube. These data are compared to performance calculations for the explosively driven shock tube in Figure 19.

Total explosive energy in the explosive driver described above is approximately 11.2 MJ. Observed energy in the driver gas, both internal and kinetic, was approximately 0.8 MJ, so that the overall thermodynamic efficiency of the explosive system is slightly greater than 7%.

ACKNOWLEDGMENTS

The shock tube research presented in this paper was possible only because of extensive previous research on the linear explosive driver. The authors are particularly appreciative of the contributions of Dr. C. S. Godfrey, Mr. E. T. Moore, Jr., Mr. J. D. Watson, Mr. G. B. Steel, and Dr. H. F. Waldron in developing the explosive driver system, and in identifying the principal nonideal phenomena affecting its performance.

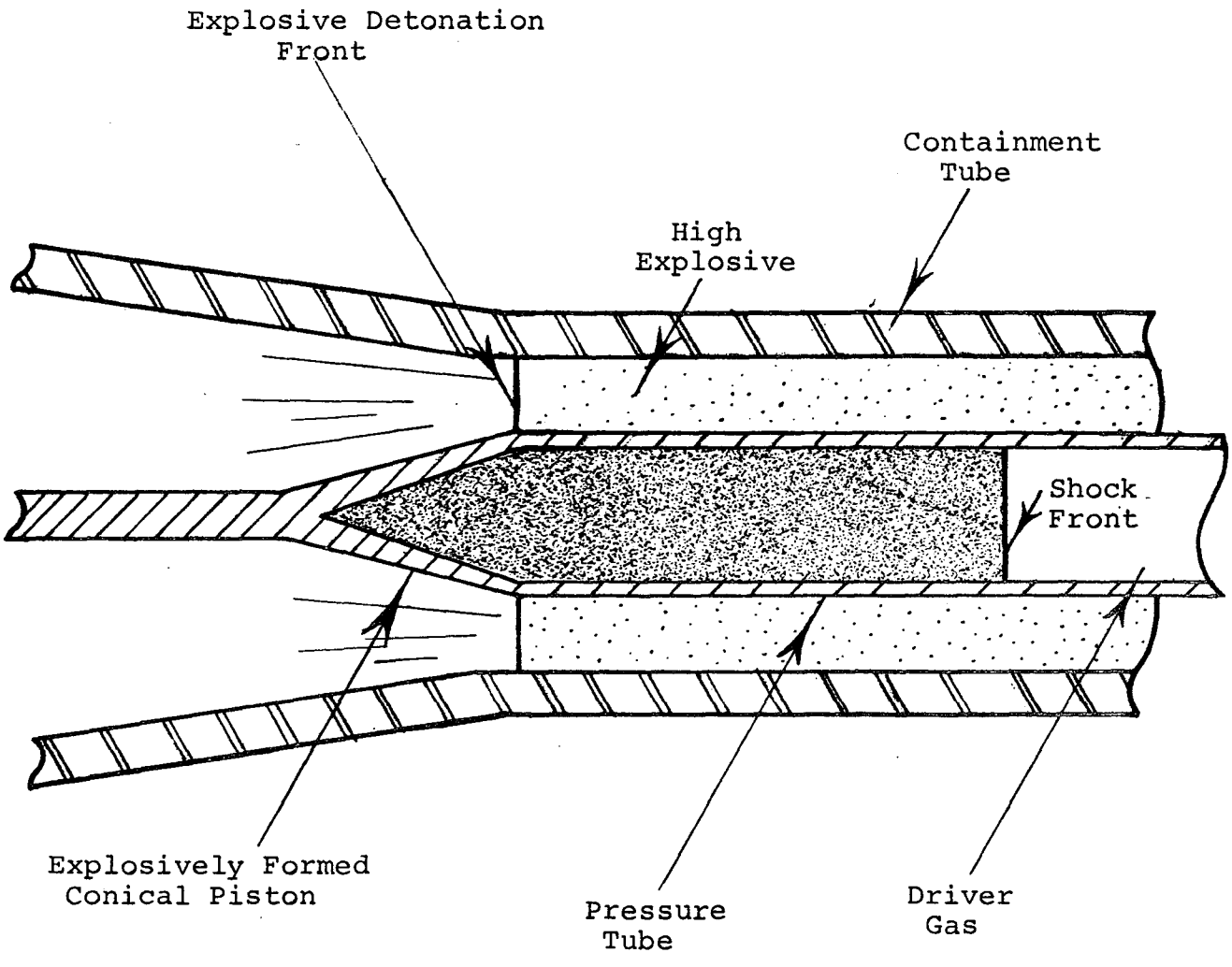

FIGURE 1. IDEALIZED SCHEMATIC OF LINEAR EXPLOSIVE DRIVER

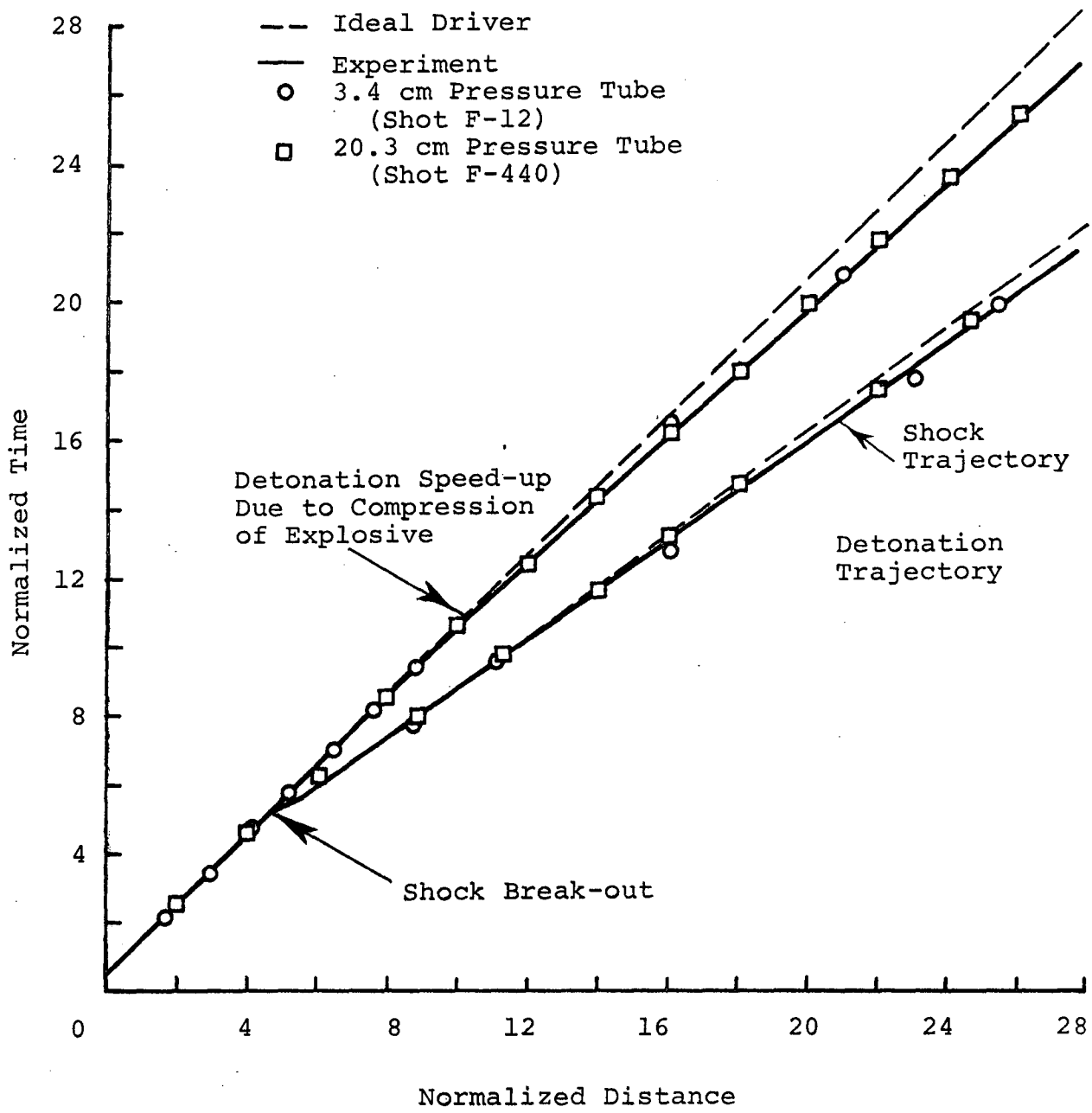

FIGURE 2. EXPLOSIVE DRIVER WAVE DIAGRAM

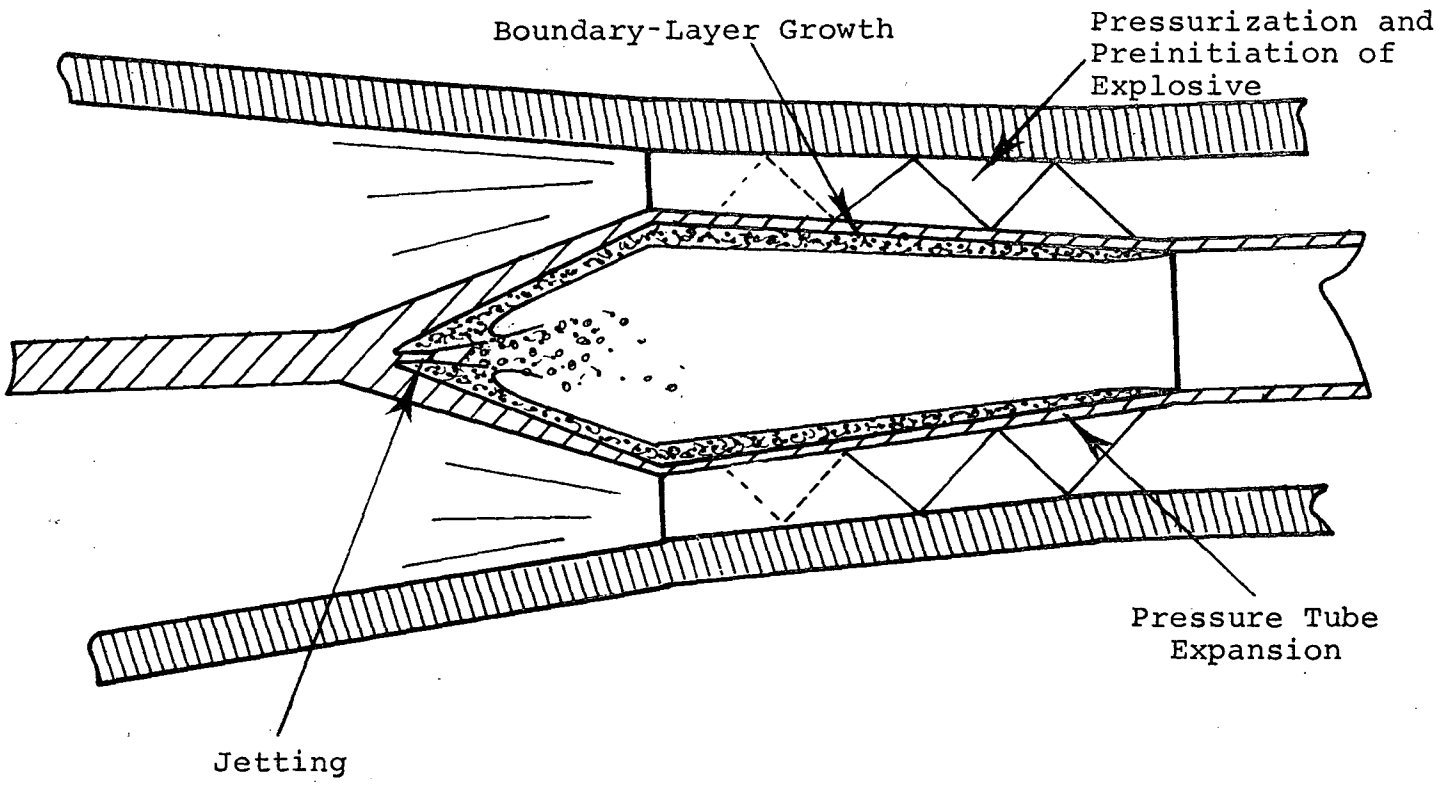

FIGURE 3. SCHEMATIC OF NONIDEAL PHENOMENA IN EXPLOSIVE DRIVERS

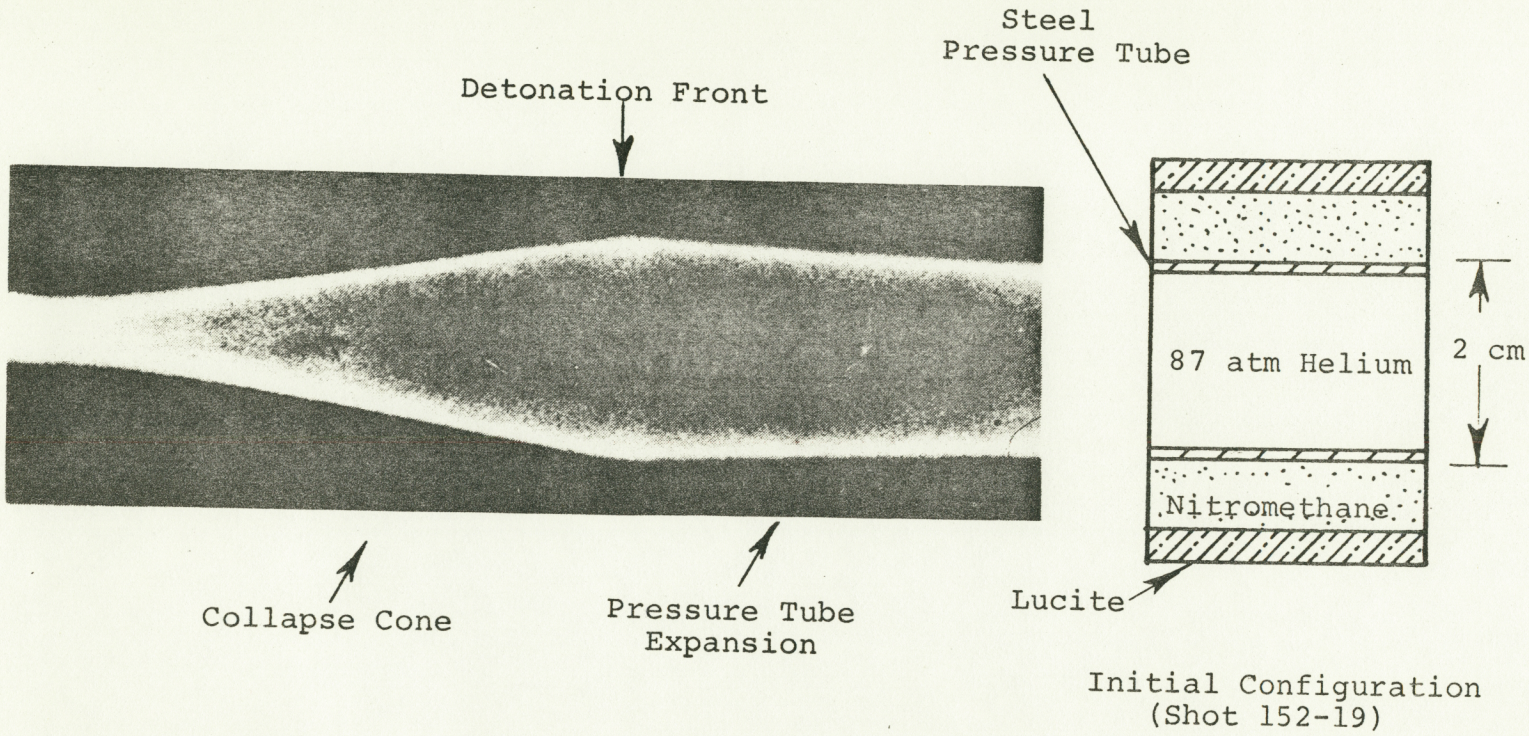

FIGURE 4. FLASH RADIOGRAPH OF EXPLOSIVE DRIVER OPERATION

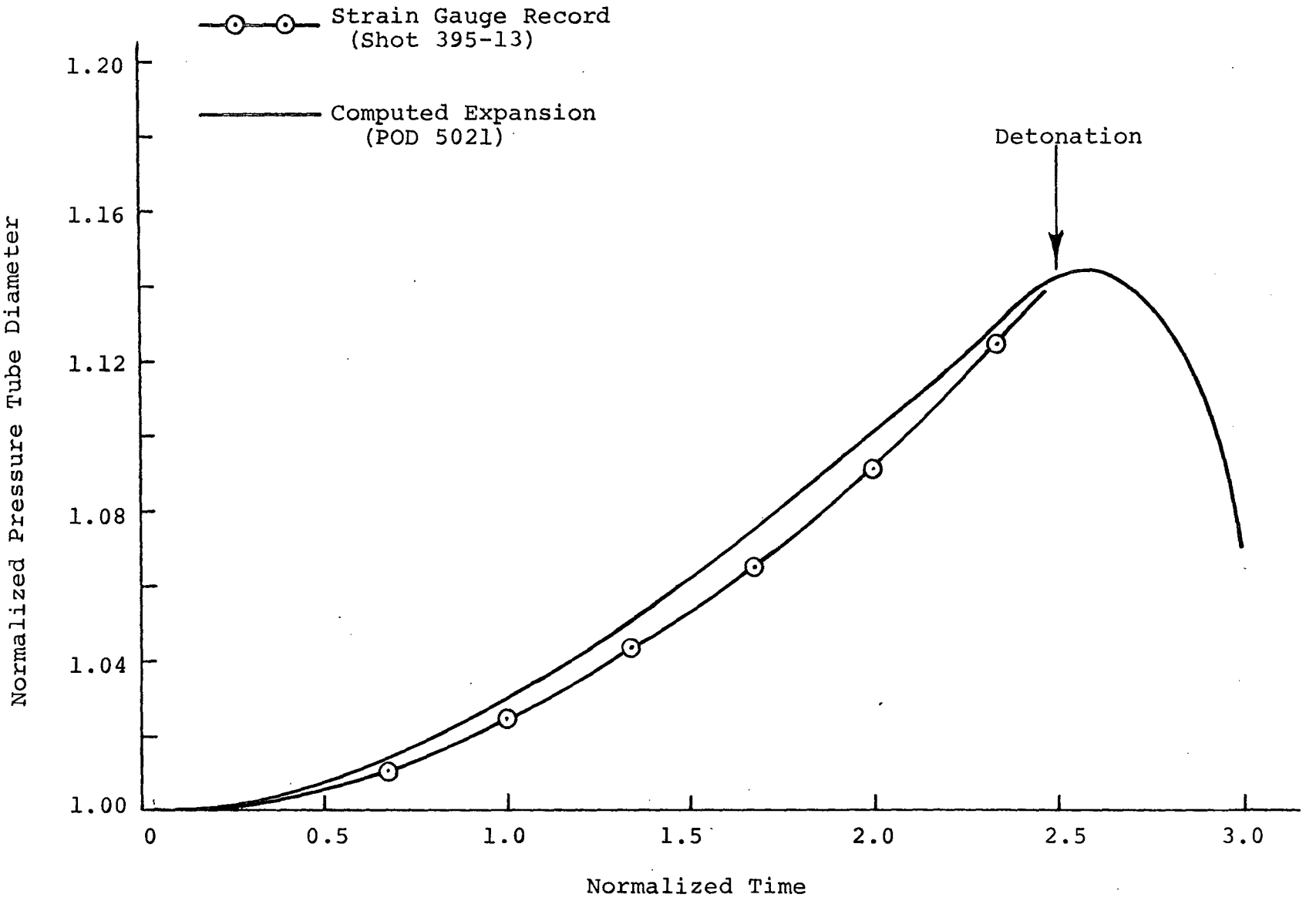

FIGURE 5. PRESSURE TUBE EXPANSION

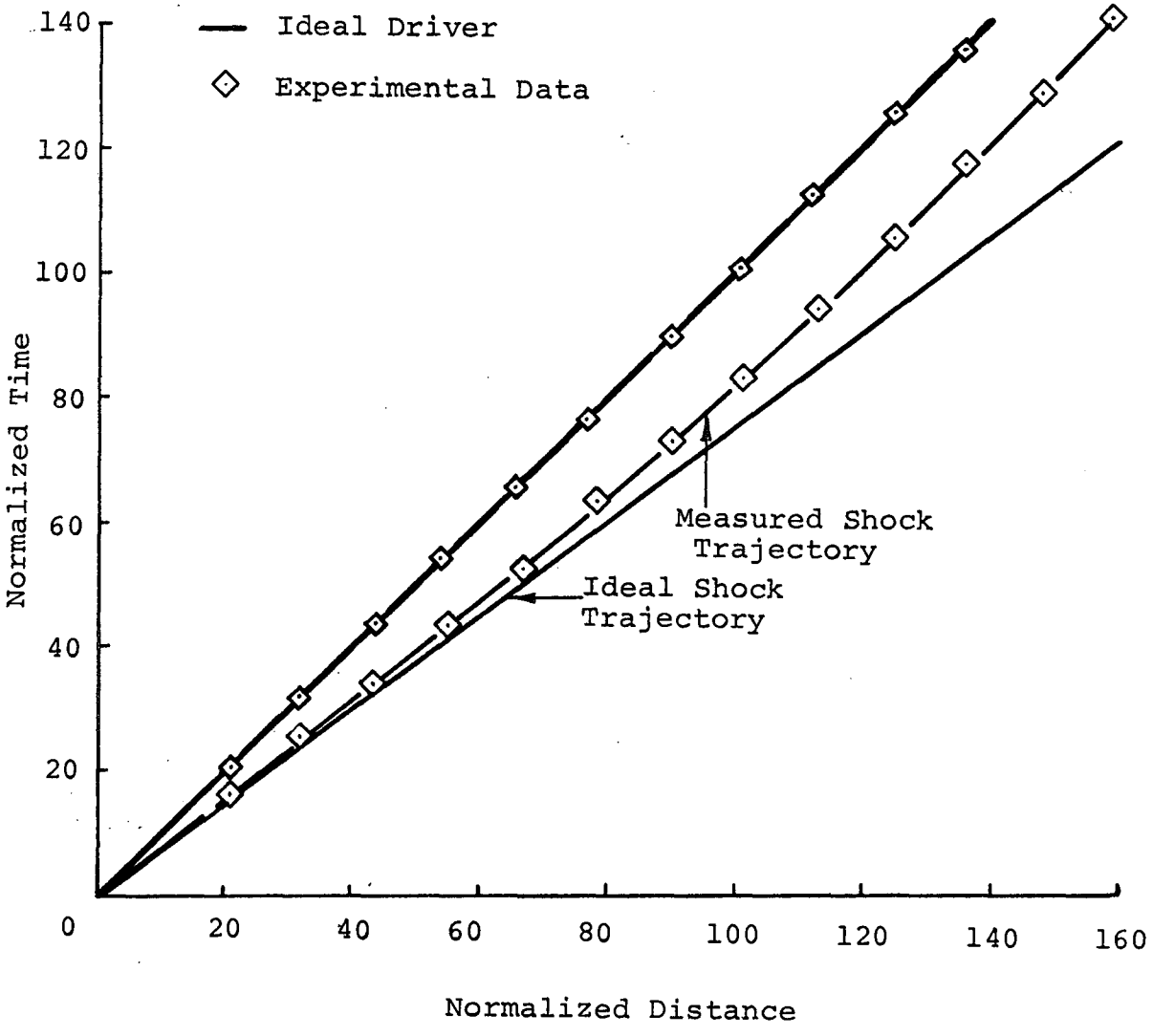

FIGURE 6. INFLUENCE OF BOUNDARY-LAYER GROWTH ON EXPLOSIVE DRIVER PERFORMANCE

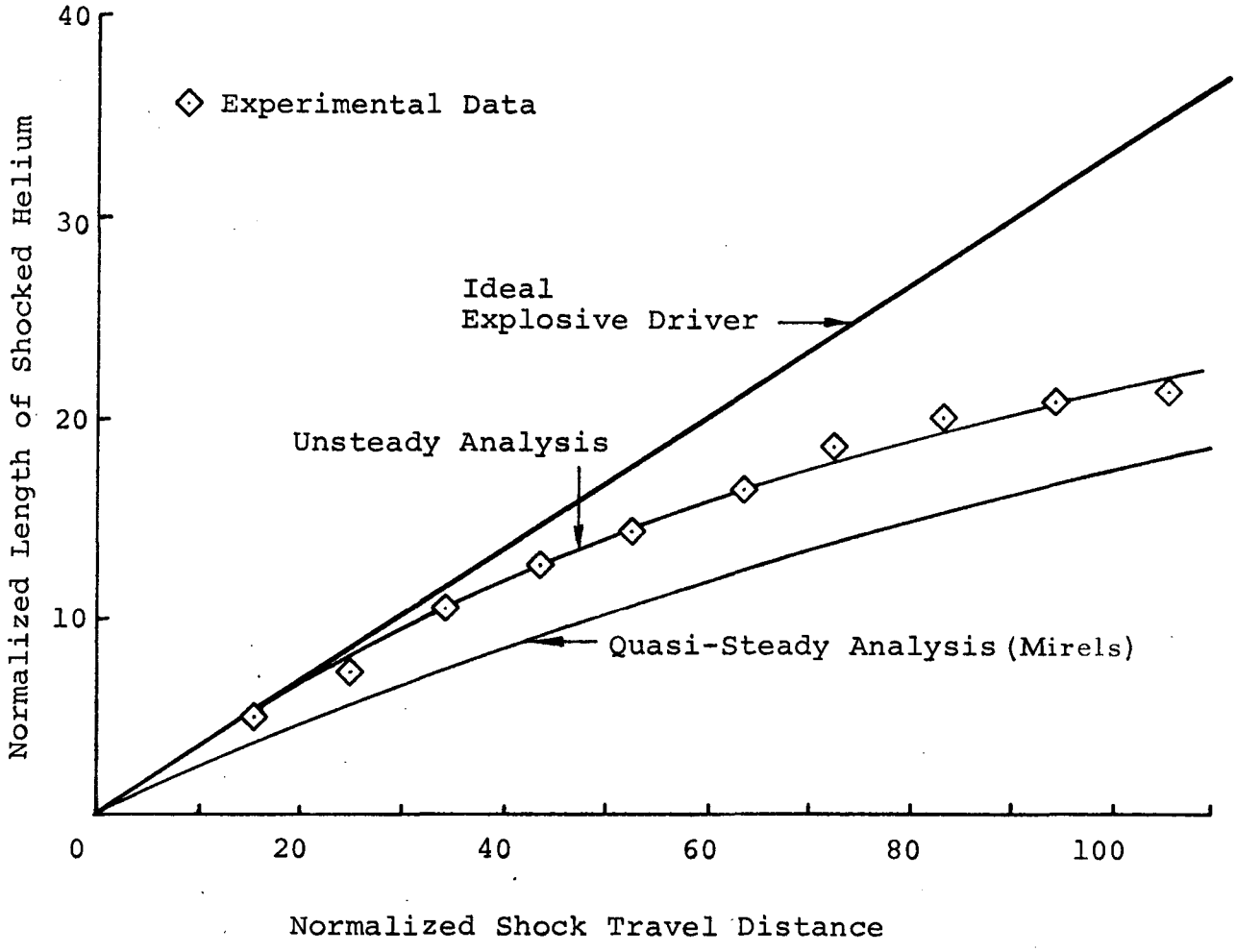

FIGURE 7. BOUNDARY-LAYER EFFECTS ON SHOCKED-GAS LENGTH

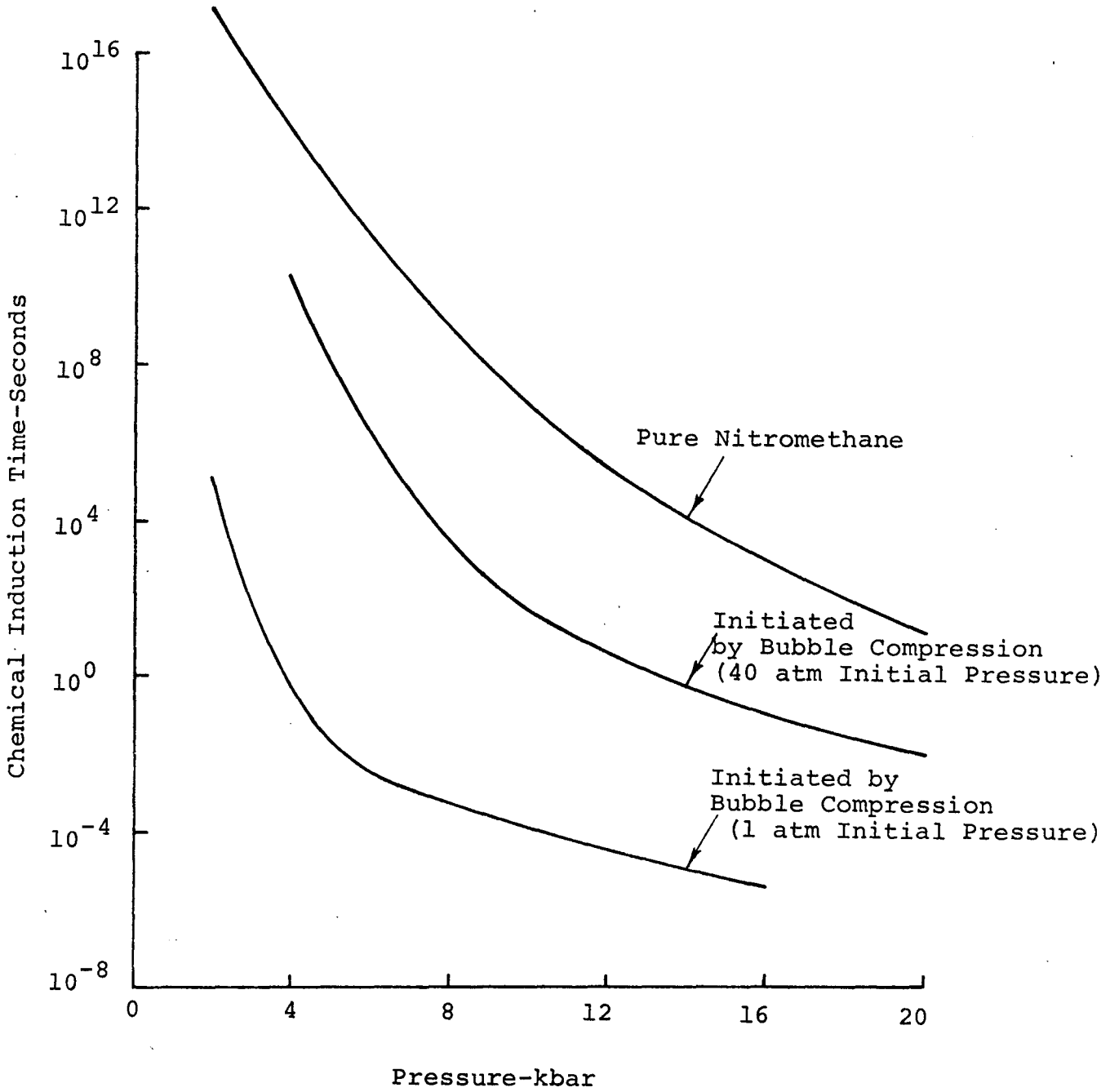

FIGURE 8. INITIATION TIMES IN NITROMETHANE AS A FUNCTION OF PRESSURE

5019

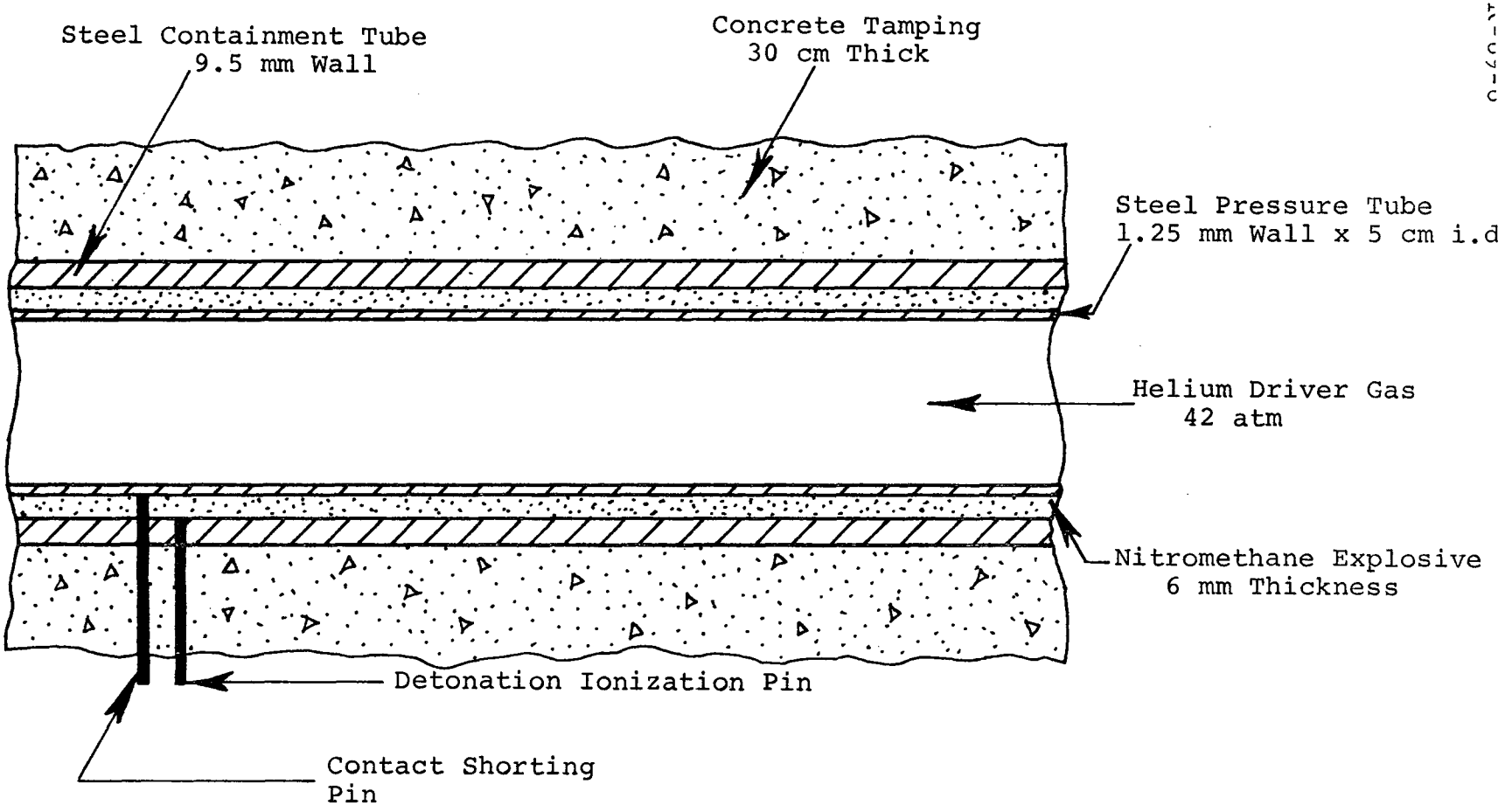

FIGURE 9. EXPLOSIVE DRIVER CONFIGURATION FOR HYPERVELOCITY SHOCK TUBE EXPERIMENTS

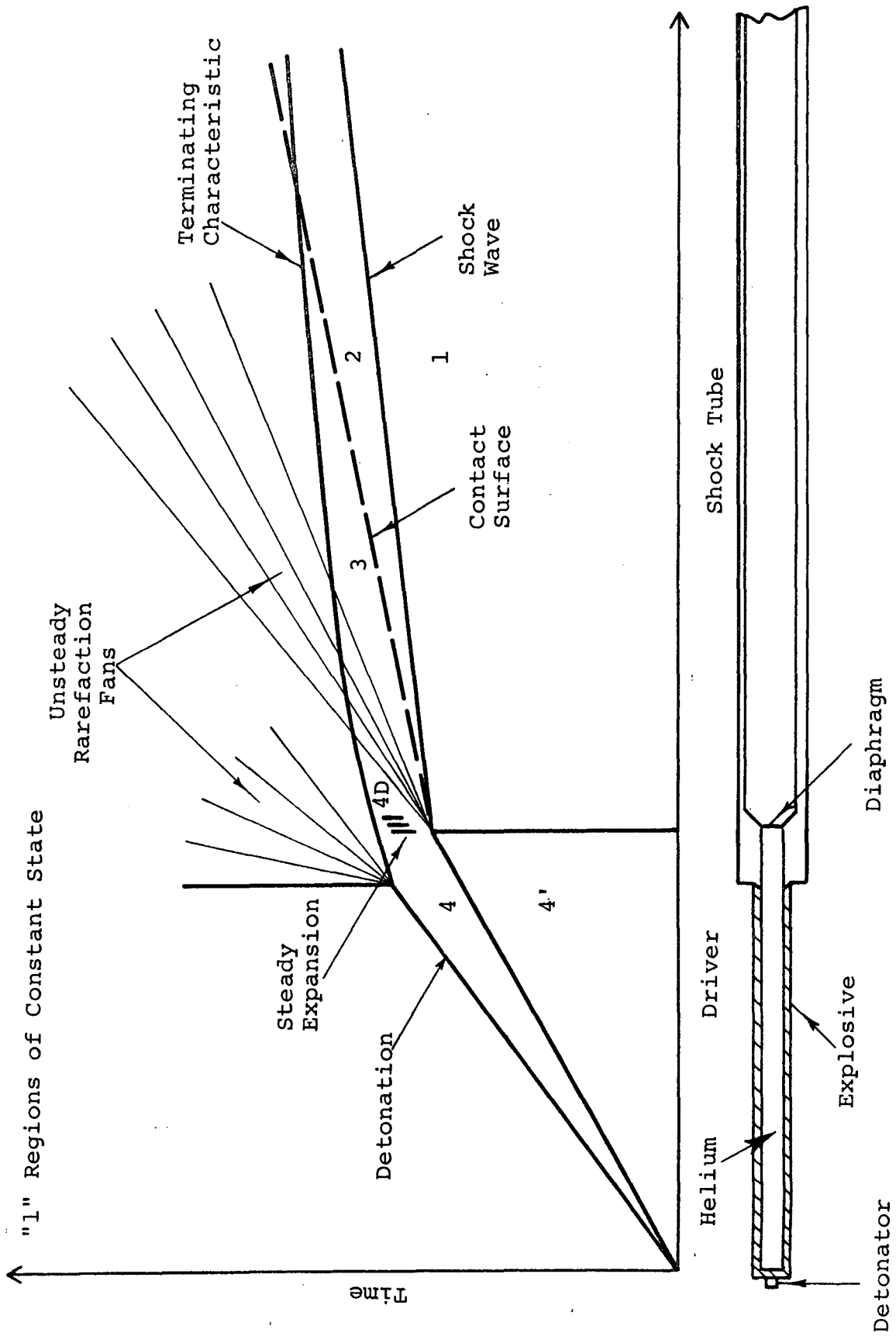

FIGURE 10. WAVE DIAGRAM OF EXPLOSIVELY DRIVEN SHOCK TUBE

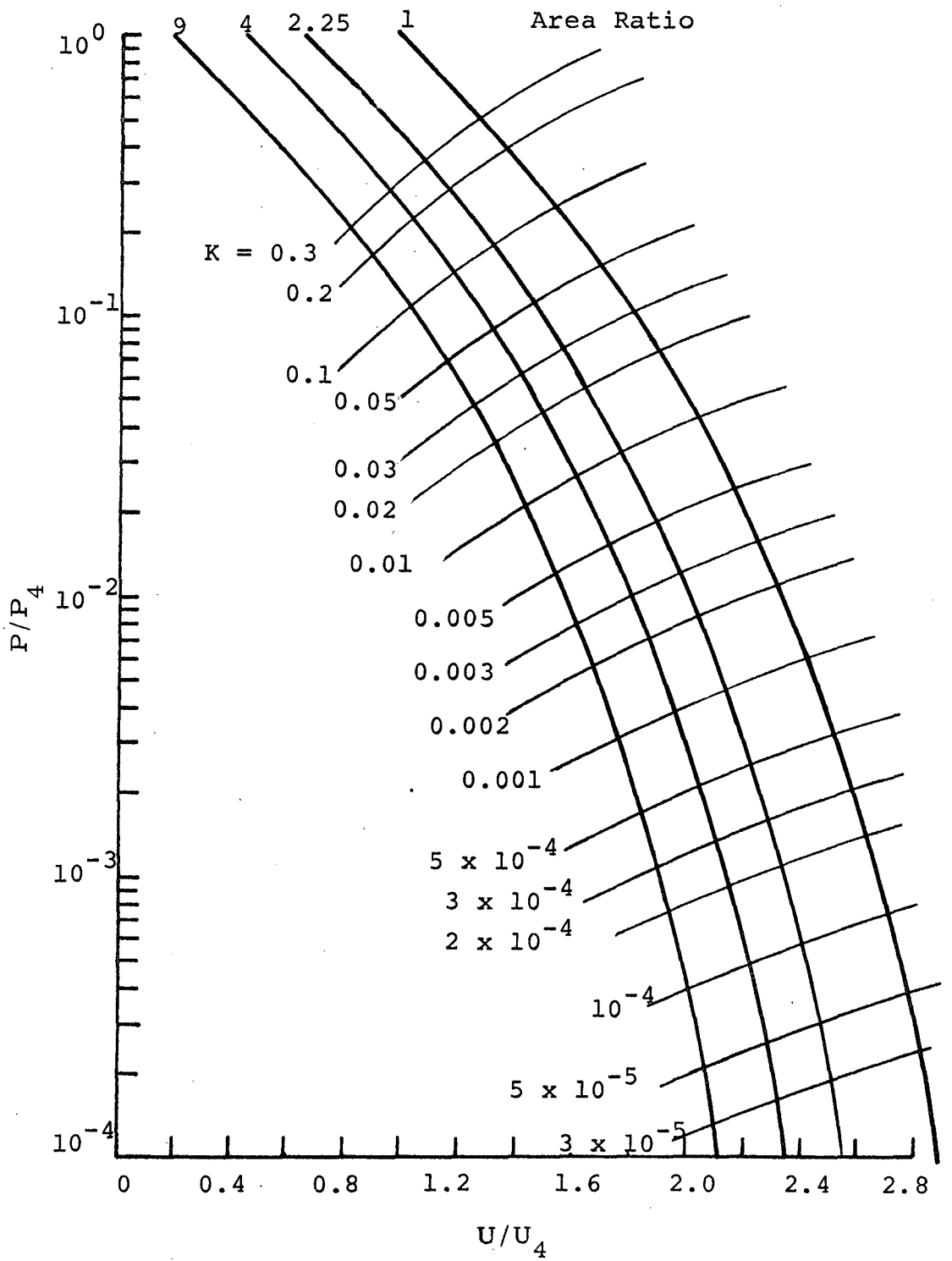

7292

FIGURE 11. PRESSURE-VELOCITY RELATIONSHIPS IN AN EXPLOSIVELY DRIVEN SHOCK TUBE

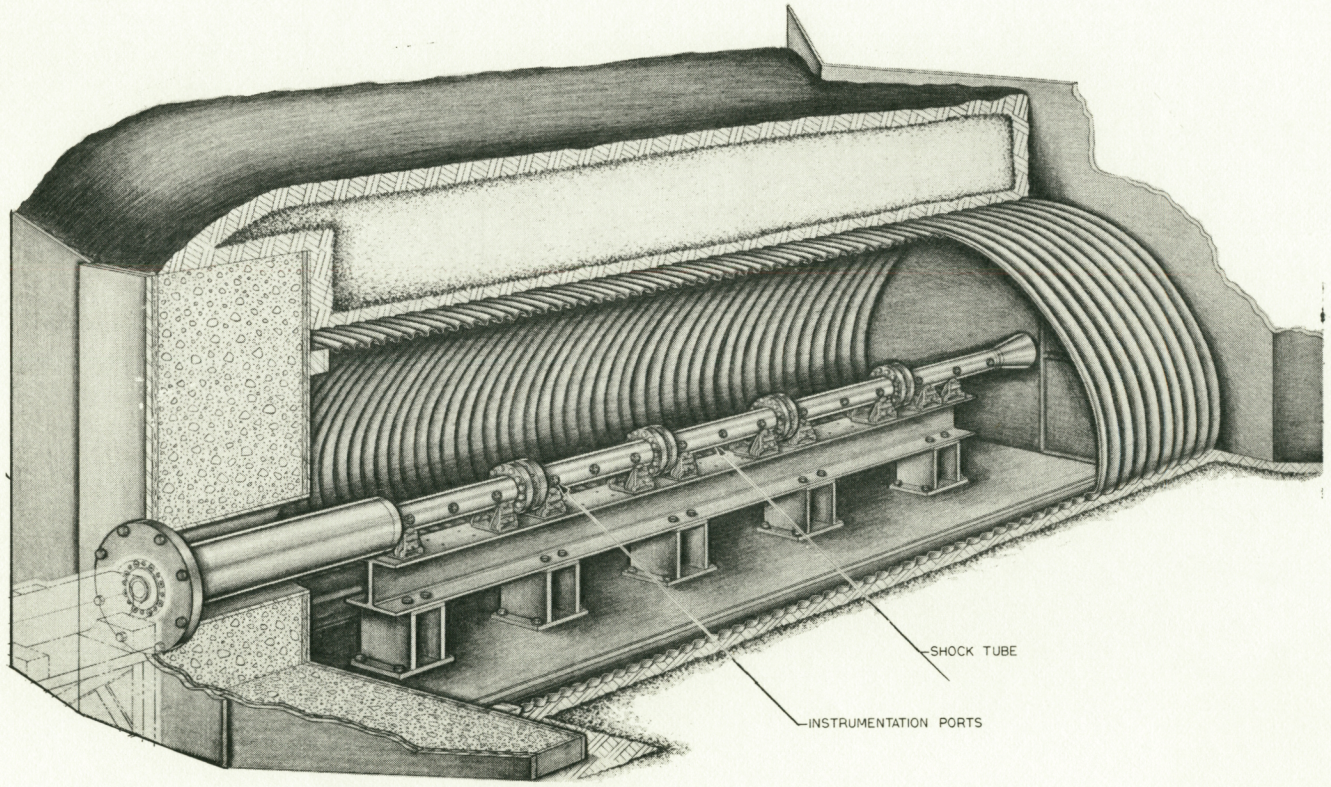

PERSPECTIVE CUT-AWAY VIEW

FIGURE 12. EXPLOSIVELY DRIVEN SHOCK TUBE LABORATORY AT PHYSICS INTERNATIONAL TRACY TEST SITE

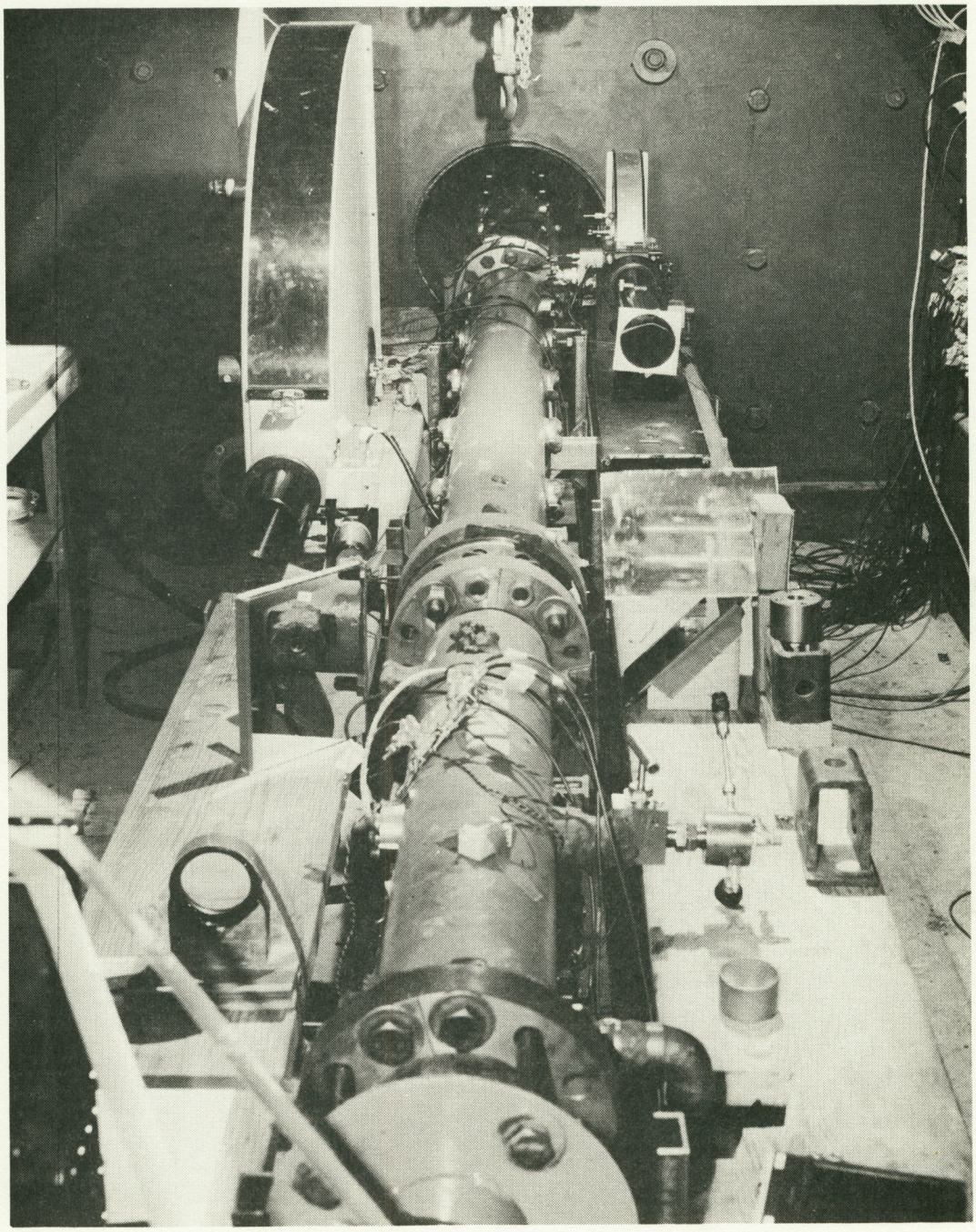

FIGURE 13. SHOCK TUBE INSTRUMENT SETUP

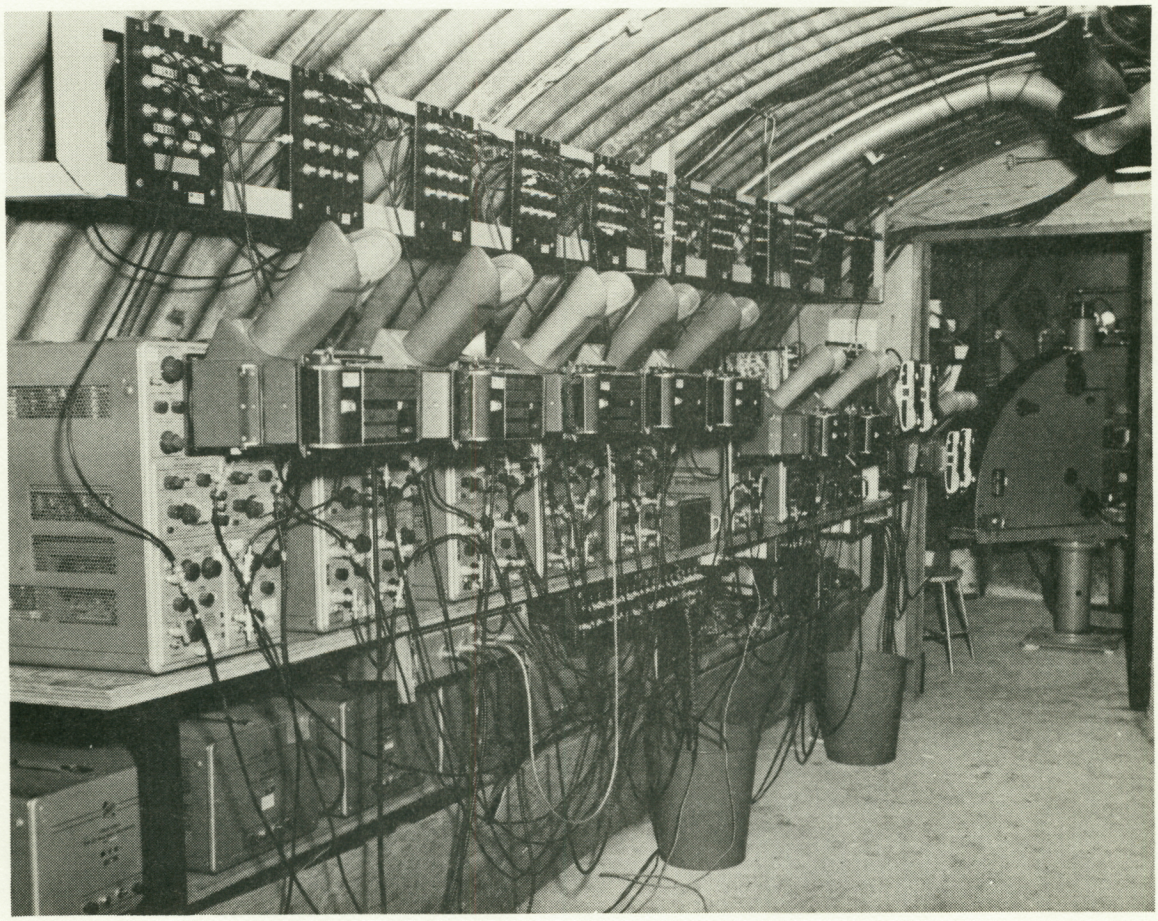

FIGURE 14. RECORDING INSTRUMENTS IN INSTRUMENTATION AND CONTROL BUNKER

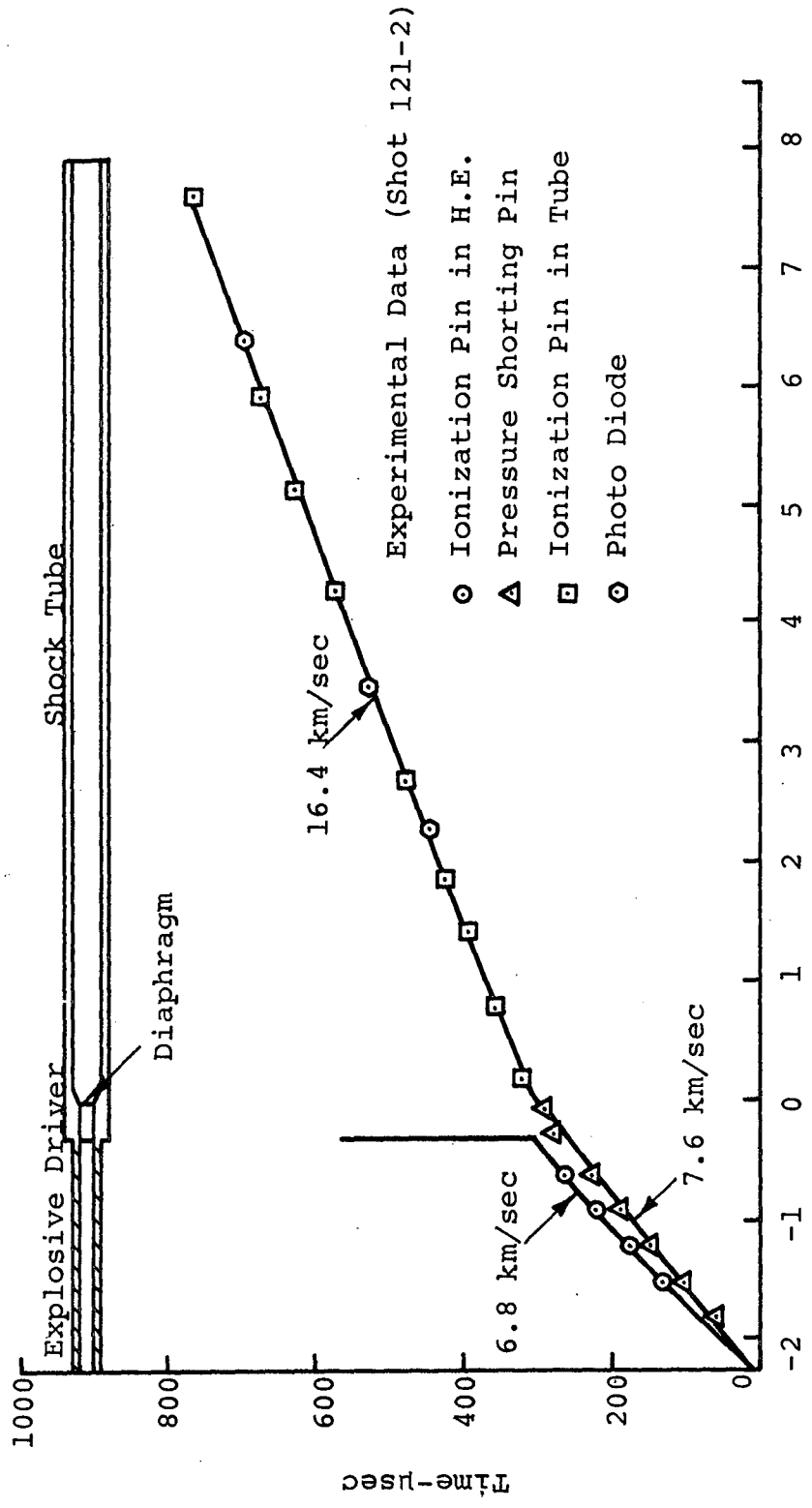

FIGURE 15. EXPERIMENTAL WAVE DIAGRAM OF EXPLOSIVELY DRIVEN SHOCK TUBE

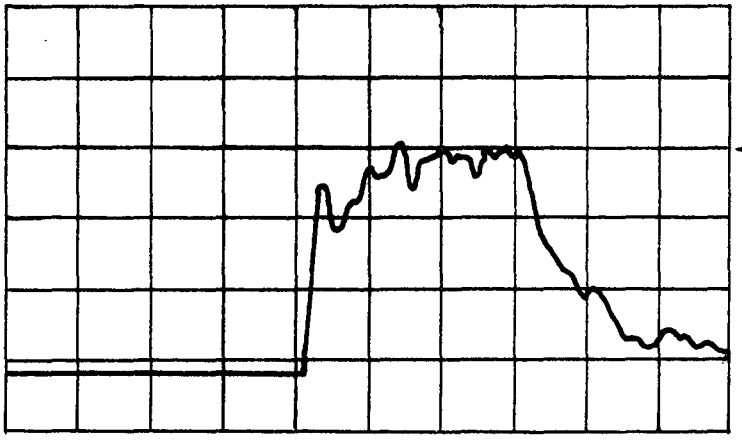

FIGURE 16. EXPLOSIVE DRIVER PRESSURE RECORD

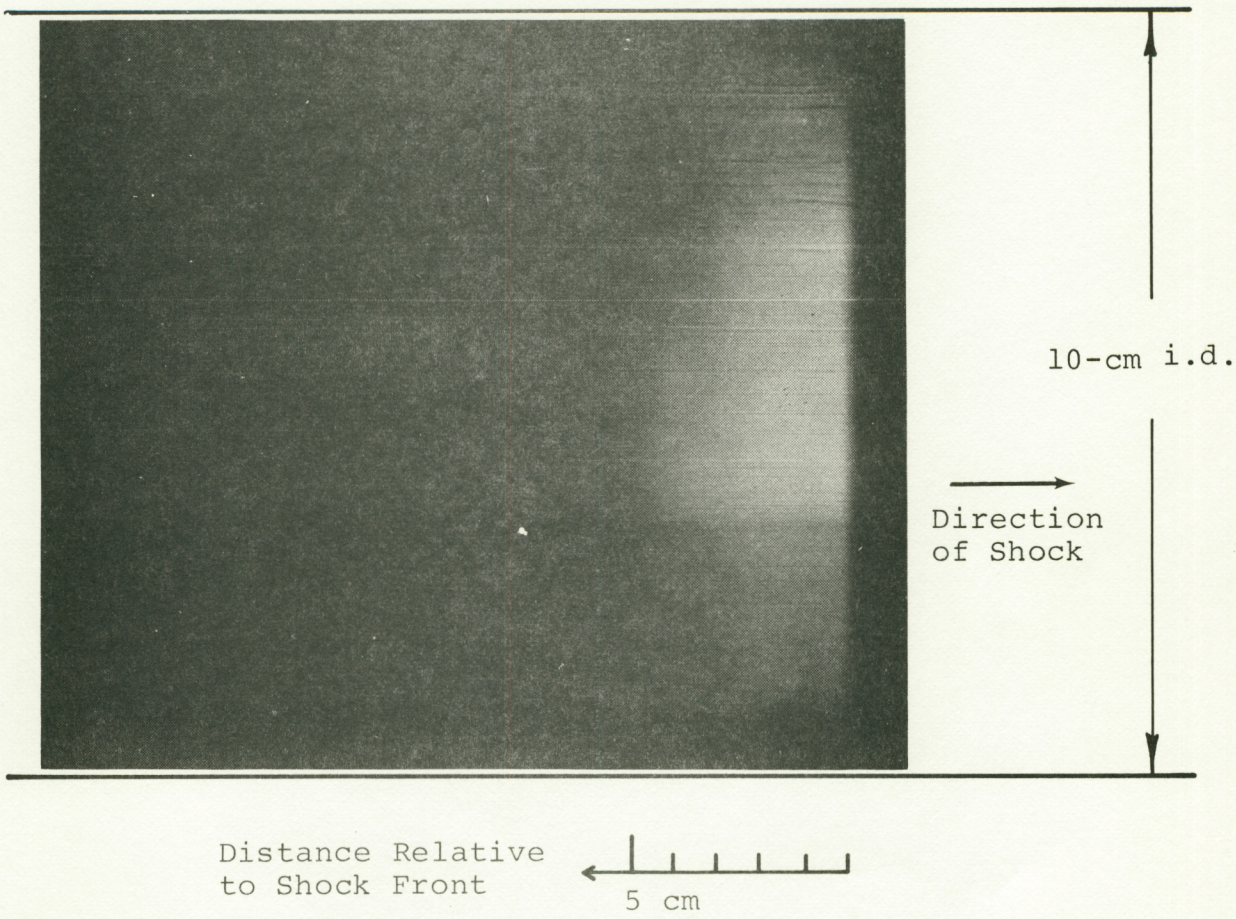

FIGURE 17. STREAKING CAMERA PHOTOGRAPH OF SHOCKED AIR

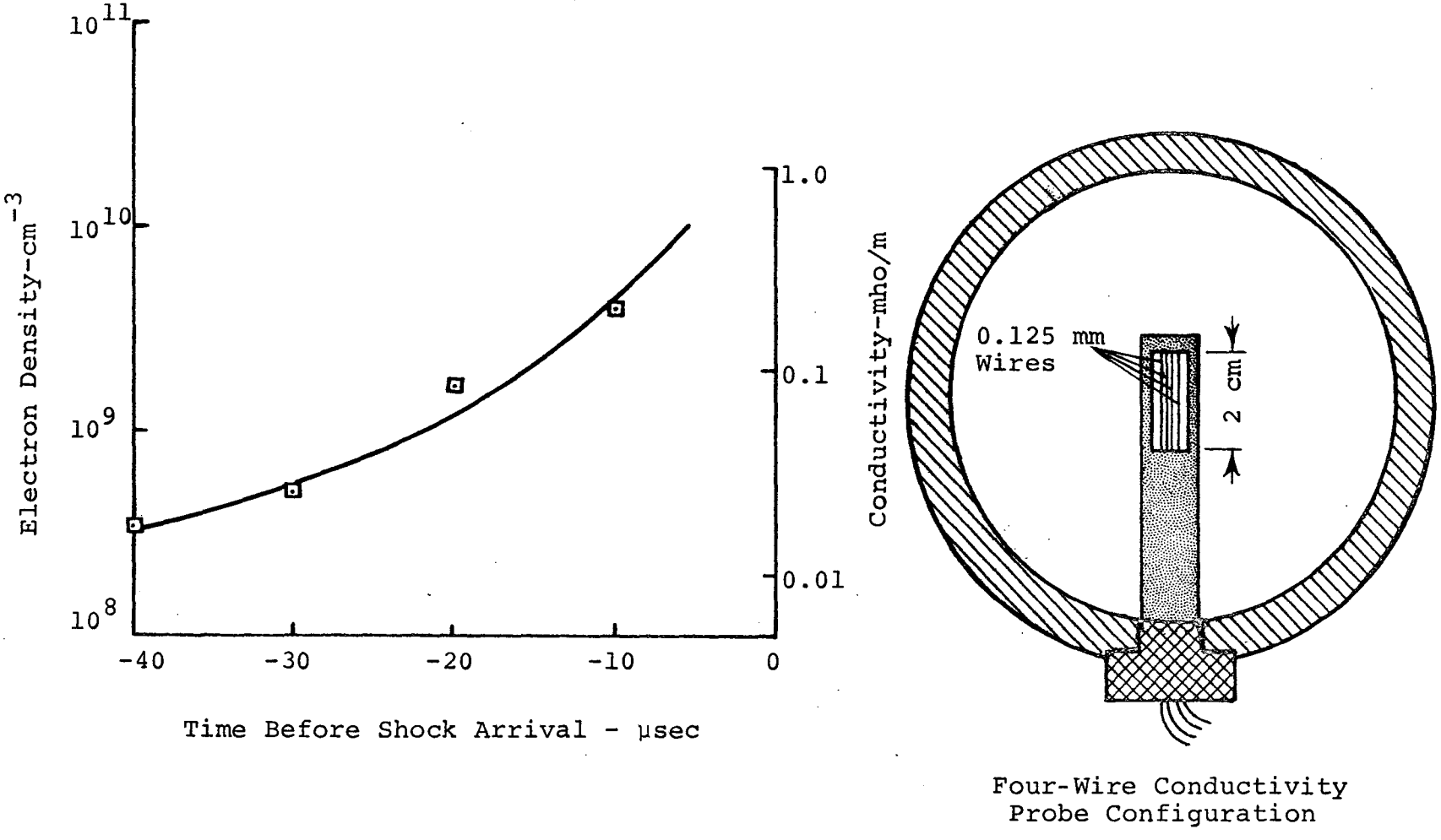

FIGURE 18. PRECURSOR CONDUCTIVITY MEASUREMENTS

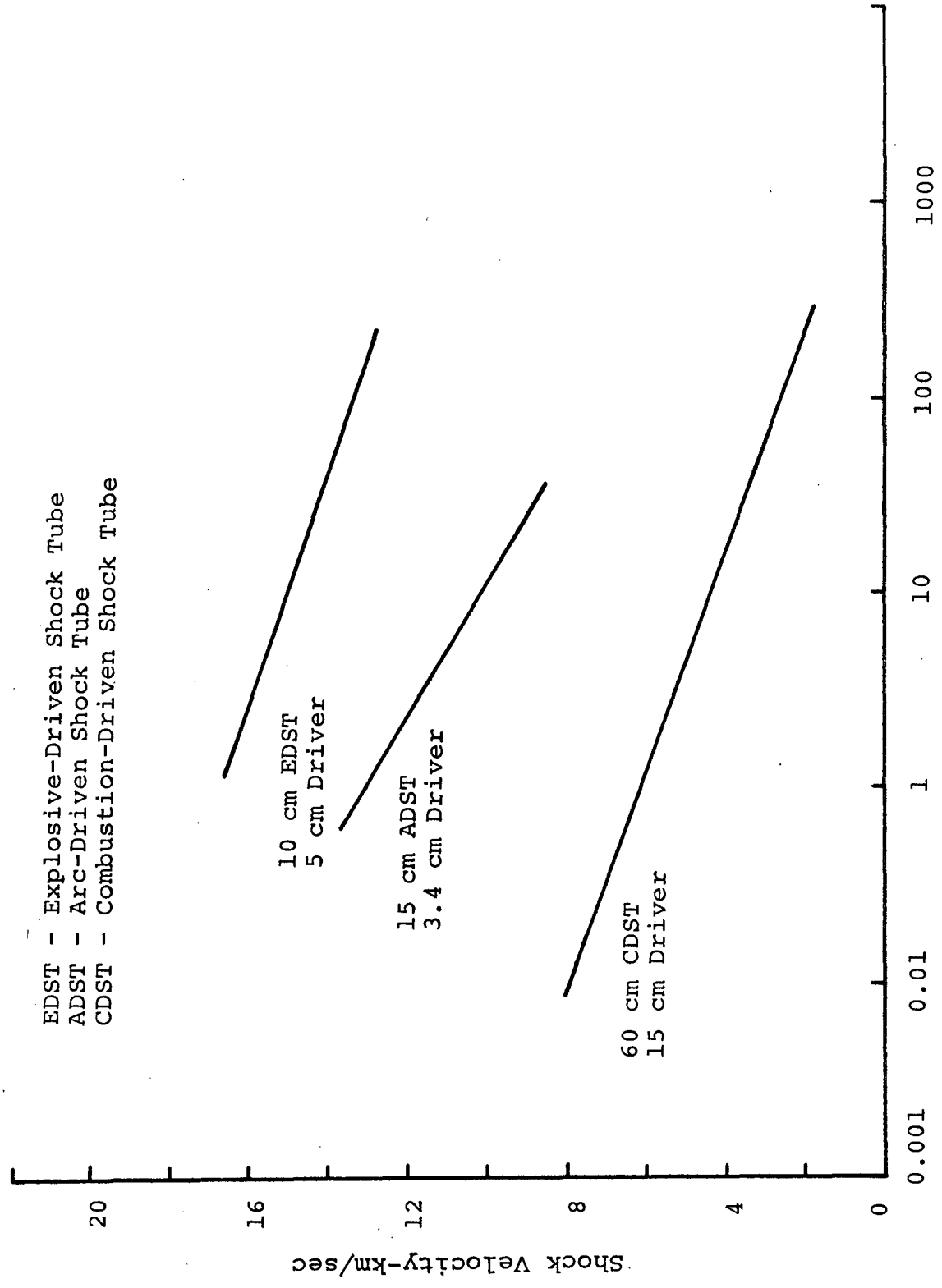

FIGURE 19. APPROXIMATE PERFORMANCE LIMITS OF EXISTING SHOCK TUBES

7291

REFERENCES

1. I. I. Glass, "Shock and Combustion Wave Dynamics in an Implosion-Driven Hypervelocity Launcher," UTIAS Review No. 25, University of Toronto, Toronto, Ontario, Canada (January 1965).

2. J. D. Watson, "Implosion-Driven Hypervelocity Launcher Performance Using Gaseous Detonation Waves," UTIAS Technical Note No. 113, University of Toronto, Toronto, Ontario, Canada (May 1967).

3. G. E. Seay, et al., J. Appl. Phys. 32, 2439 (1961).

4. A. E. Voitenko, Sov. Phys. Doklady 9, 860 (1965).

5. A. E. Voitenko, Sov. Phys.-Tech. Phys. 11, 128 (1966).

6. A. E. Voitenko, I. Sh. Model', and I. S. Samodelov, Sov. Phys. Doklady 11, 596 (1967).

7. Yu. A. Zatsepin, E. G. Popov, and M. A. Tsikulin, Sov. Phys. JETP 27, 63 (1968).

8. V. M. Titov, Yu. I. Fadeyenko, and N. S. Titova, Letters of the Acad. of Sci. USSR 180, 1051 (1961) (in Russian).

9. S. P. Gill, "Shock Tube With Implosive Jet Driver," Phys. Fluids Supplement, to be published in 1969.

10. E. T. Moore, Jr., "Explosively Driven Shock Tubes," AEDC-TR-66-238, Arnold Engineering Development Center, Arnold Air Force Station, Tennessee (November 1966).

11. H. F. Waldron, E. T. Moore, Jr., G. B. Steel, and C. S. Godfrey, "A Mechanism for the Conversion of the Chemical Energy of Explosives to the Kinetic and Internal Energy of a Gas," AIAA Paper No. 67-178, presented at the AIAA Fifth Aerospace Sciences Meeting, New York, New York (January 1967).

12. S. P. Gill, "Implosively Driven Shock Tubes," Poulter Laboratories Technical Report No. 001-66, Stanford Research Institute, Menlo Park, California (December 1966).

13. H. Mirels, "Shock Tube Test Time Limitation Due to Turbulent-Wall Boundary Layer," AIAA J. 2, 84 (January 1964).

14. J. W. Enig and F. J. Petrone, "An Equation of State and Derived Shock Initiation Criticality Conditions for Liquid Explosives," 4th Detonation Symposium, U. S. Naval Ordnance Laboratory, White Oak, Silver Spring, Maryland (October 12, 1965).

15. G. Birkhoff, D. P. MacDougall, E. M. Pugh, and G. I. Taylor, "Explosives With Lined Cavities," J. Appl. Phys. 19, 563 (June 1948).

16. "Equations, Tables, and Charts for Compressible Flow," Report No. 1135, National Advisory Committee for Aeronautics, Washington, D. C. (1953).

17. R. Courant and K. O. Friedricks, Supersonic Flow and Shock Waves, Interscience (1948), p. 104 ff.

18. R. T. Brown and M. Mitchener, "Measurements in a Two-Temperature Plasma Boundary Layer," AIAA Paper No. 69-692, AIAA Fluid and Plasma Dynamics Conference, San Francisco, California (June 1969).

19. See, for example, D. J. Rose and M. Clark, Jr., Plasmas and Controlled Fusion (MIT Press, 1961) p. 147.

20. J. C. Camm and P. H. Rose, Phys. Fluids 6, 663 (1963).